



TECHNISCHE
UNIVERSITÄT
WIEN
Vienna | Austria

Diploma Thesis

Combustion of Hydrocarbon and Alternative Fuels in Non-premixed Flows

carried out for the purpose of obtaining the degree of Dipl.-Ing.,
submitted at TU Wien, Faculty of Mechanical and Industrial Engineering, by

Simon Leu

Student ID Number: 01426711

under the supervision of

Ao.Univ.Prof.i.R. Dipl.-Ing. Dr.techn. Ernst Pucher

Institute for Powertrains and Automotive Technology

TU Wien, Austria

and

Prof. Dr. Kalyanasundaram Seshadri

Department of Mechanical and Aerospace Engineering

University of California, San Diego, USA

Abstract

In view of strict environmental restrictions imposed by governments, especially for vehicles with internal combustion engines, combustion research is essential. Although the number of electric vehicles is steadily increasing, most vehicles on the road are still powered by internal combustion engines.

The research in this field should lead to a better understanding, description, and prediction of combustion processes. Additionally, it could improve the efficiency of existing internal combustion engines and assist in developing alternative fuels and renewable energy sources.

In this diploma thesis, selected aspects of the combustion of hydrocarbon fuels and alternative fuels, more precisely pure ethanol, mixtures of ethanol with decane, and pure decane, are investigated experimentally in non-premixed flows. The critical conditions of autoignition and extinction are examined more closely for these fuels. The conducted experiments provide autoignition temperatures as a function of the strain rate and strain rates as a function of the oxygen mass fraction of the oxidizer stream at extinction. The experiments employ the counterflow burner developed at the University of California, San Diego. Counterflow burners are commonly used devices for combustion research in many laboratories.

The experimental results are compared with the results from a numerical simulation to identify whether there is a discrepancy or other anomalies.

For the investigation of the autoignition temperatures, the experimental and numerical results have a similar trend: Increasing the strain rate makes the fuels harder to ignite, and the autoignition temperature increases.

The results also indicate the higher the decane share is in the mixture, the higher is the autoignition temperature, especially at lower strain rates.

The mixtures of ethanol and decane indicate a previously unknown behavior at lower strain rates: Mixtures with a small share of ethanol are harder to ignite in the experiments than the numerical results predict. It seems that already small shares of ethanol in the mixtures inhibit the low-temperature chemistry of decane.

During the simulation of the numerical extinction results, it has been observed that the used mechanism does not support the calculation of the extinction strain rates of liquid fuels. Consequently, the investigation of extinction in this work can only focus on the experimental results.

The experimental extinction results show that the higher the oxygen mass fraction of the oxidizer stream, the higher is the extinction strain rate, regardless of the fuel.

Additionally, the results show that the strain rate increases at a constant oxygen mass fraction of the oxidizer stream with higher ethanol content in the fuel.

Kurzfassung

Angesichts der strengen Umweltauflagen seitens der Regierungen, insbesondere für Fahrzeuge mit Verbrennungsmotoren, ist die Forschung im Bereich der Verbrennung unerlässlich. Obwohl die Anzahl der Elektrofahrzeuge jedes Jahr zunimmt, werden die meisten Fahrzeuge auf den Straßen immer noch von klassischen Verbrennungsmotoren angetrieben.

Ziel der Forschung auf diesem Gebiet ist es, Verbrennungsprozesse besser verstehen, beschreiben und vorhersagen zu können. Außerdem kann mit dem gewonnenen Wissen die Effizienz bestehender Verbrennungsmotoren verbessert und die Entwicklung nach alternativen Kraftstoffen und erneuerbaren Energiequellen unterstützt werden.

In dieser Diplomarbeit werden ausgewählte Aspekte der Verbrennung von Kohlenwasserstoff-Kraftstoffen und alternativen Kraftstoffen in nicht vorgemischten Strömungen experimentell untersucht. Bei den getesteten Kraftstoffen handelt es sich um reines Ethanol, Mischungen von Ethanol mit Decan und reines Decan. Dabei werden die kritischen Bedingungen der Selbstzündung und der Auslöschung von den oben genannten Kraftstoffen näher untersucht. Bei den Experimenten werden Selbstentzündungstemperaturen in Abhängigkeit von der Strain-Rate und die Strain-Rate in Abhängigkeit vom Sauerstoffmassenanteil des Oxidationsmittelstroms bei Auslöschung ermittelt. Für die Experimente wird ein Gegenstrombrenner, welcher an der University of California, San Diego entwickelt wurde, verwendet. Dies ist ein häufig verwendetes Instrument in der experimentellen Verbrennungsforschung.

Die experimentellen Ergebnisse werden mit den Ergebnissen einer numerischen Simulation verglichen. Der Vergleich der experimentellen und numerischen Ergebnisse soll zeigen, ob es Diskrepanzen oder andere Anomalien zwischen den beiden Datensätzen gibt.

Bei der Untersuchung der Selbstentzündungstemperaturen weisen die experimentellen und numerischen Ergebnisse einen ähnlichen Trend auf: Mit zunehmender Strain-Rate sind die Kraftstoffe schwerer zu entzünden und die Selbstentzündungstemperatur steigt an.

Die Ergebnisse zeigen auch, dass die Selbstentzündungstemperatur umso höher ist, je höher der Decan-Anteil im Gemisch ist, insbesondere bei niedriger Strain-Rate.

Bei der Analyse der Gemische aus Ethanol und Decan zeigt sich bei niedriger Strain-Rate ein bisher unbekanntes Verhalten: Gemische mit einem geringen Ethanol-Anteil sind in den Experimenten schwerer zu entzünden, als es die numerischen Ergebnisse prognostizieren. Es scheint, dass bereits geringe Anteile von Ethanol in den Gemischen die Niedertemperaturchemie von Decan hemmen.

Bei der Simulation der numerischen Auslöschungsergebnisse wurde festgestellt, dass der verwendete Mechanismus die Berechnung der Auslöschungs-Strain-Rate von flüssigen Kraftstoffen nicht unterstützt. Daher enthalten die Untersuchungen zur Auslöschung in dieser Arbeit nur experimentelle Ergebnisse.

Die experimentellen Auslöschungsergebnisse zeigen, dass die Auslöschungs-Strain-Rate unabhängig vom Brennstoff umso höher ist, je höher der Sauerstoffmassenanteil des Oxidationsmittelstroms ist.

Zudem zeigen die Ergebnisse, dass die Strain-Rate bei konstantem Sauerstoffmassenanteil des Oxidationsmittelstroms mit höherem Ethanol-Anteil im Kraftstoffgemisch zunimmt.

Acknowledgments

“Patience is a key element of success.”

Bill Gates

In so many aspects of my diploma thesis, patience was indeed the key element of success – in the run-up, to keep cool due to all the postponements regarding the pandemic, and during the diploma thesis, to perform the experiments accurately. The whole time of my diploma thesis, I have experienced a great deal of support and assistance.

First and foremost, I would like to express my deepest appreciation to Professor Pucher from TU Wien, who offered me this unique opportunity to write my diploma thesis in California. Also, I cannot overestimate his help both before and during my work.

I am extremely grateful to have such a supervisor as Professor Seshadri from the University of California, San Diego. With his unparalleled combustion knowledge and practical suggestions, he was a tremendous help to me throughout my time in California.

Furthermore, I also had the great pleasure of working with Liang Ji in the laboratory. He supported me with helpful advice during the experimental part of my diploma thesis.

Additionally, I would like to acknowledge the Austrian Marshall Plan Foundation. I feel very honored to have been selected for the Marshall Plan Scholarship Program.

Thanks also to my study colleagues who became friends over the years of study. Without you, the studies would never have been possible.

Finally, I’m extremely grateful for the unrelenting support and continuous encouragement of my family. They always have profound beliefs in my abilities. Therefore, I dedicate this final step of my studies to them.

San Diego, September 2021

Simon

Contents

List of Abbreviations and Symbols	I
1 Introduction	1
2 Fundamentals of Combustion Theory and Theoretical Framework	3
2.1 Autoignition, Extinction, and Diffusion Flame.....	3
2.2 General Information on Hydrocarbons.....	6
2.2.1 Ethanol	7
2.2.2 Decane	8
2.3 Strain Rate, Damköhler Number, and S-shaped Curve	9
3 Experimental Setup and Procedure	13
3.1 Experimental Setup for Autoignition and Extinction	13
3.1.1 Counterflow Burner	14
3.1.2 Liquid Supply System.....	19
3.1.3 Gas Supply and Control System	19
3.1.4 Temperature Measurement	20
3.1.5 Control Software	21
3.1.6 Exhaust System.....	22
3.2 Procedures for Autoignition and Extinction Experiments.....	22
4 Experimental and Numerical Results	26
4.1 Experimental Results.....	26
4.2 Numerical Results	33
4.3 Comparison and Discussion of Experimental and Numerical Results	35
5 Conclusions	41
Appendix.....	i
References	vii
List of Equations	x
List of Figures	xi
List of Tables.....	xiii
Affidavit.....	xiv

List of Abbreviations and Symbols

a_2	Oxidizer strain rate	1/s
d	Diameter thermocouple	m
Da	Damköhler number	-
Da_I	Damköhler number at ignition	-
Da_E	Damköhler number at extinction	-
h	Convective heat transfer coefficient	W/m ² K
k	Thermal conductivity	W/mK
L	Separation distance	m
Nu	Nusselt number	-
$Nu_{d,cyl}$	Nusselt number for cylindric problems	-
Re	Reynolds number	-
T_1	Temperature of fuel stream at boundary	K
T_2	Temperature of oxidizer stream at boundary	K
T_∞	Temperature of free stream of oxidizer gas	K
T_a	Average temperature of thermocouple and oxidizer gas	K
T_{ad}	Adiabatic flame temperature	K
T_g	Gas temperature	K
T_{max}	Maximum reaction temperature	K
T_{tc}	Temperature of thermocouple	K
T_w	Temperature of surroundings	K
t_D	Diffusion time	s
t_R	Reaction time	s
V_1	Flow velocity of fuel stream at boundary	m/s
V_2	Flow velocity of oxidizer stream at boundary	m/s
ϵ_{tc}	Emissivity of Type R thermocouple	-
ν	Viscosity of oxidizer stream	m ² /s
ρ_1	Density of fuel stream at boundary	kg/m ³
ρ_2	Density of oxidizer stream at boundary	kg/m ³
σ	Stefan-Boltzmann constant	W/m ² K ⁴

C	Carbon
C ₂ H ₆ O	Ethanol
C ₂ H ₆	Ethane
C ₁₀ H ₂₂	Decane
H	Hydrogen
N ₂	Nitrogen
O	Oxygen
-OH	Hydroxy group
exp.	Experimental
num.	Numerical

1 Introduction

Combustion and fossil fuels have become an integral part of today's world. Especially in the field of mobility and transportation, combustion and fossil fuels are indispensable. Although the number of alternative-powered vehicles is increasing, particularly the share of electric-powered vehicles, most vehicles are still equipped with an internal combustion engine that runs on fossil fuels.

In 2020, the global sales of electric cars increased by 41 percent to about 3 million electric cars. However, according to the International Energy Agency, this is only a 4.6 percent share of the new vehicle market [1].

In addition, there are hundreds of millions of vehicles with internal combustion engines on the roads that have been produced in recent years. Consequently, the lion's share of vehicles consists of vehicles with internal combustion engines. With their generated pollutants, all these cars have an enormous impact on the environment and threaten people's health.

To protect the environment and people's health, governments are introducing ever stricter restrictions for emissions, especially for vehicles, for example, the European emission standards or the United States vehicle emission standards.

Therefore, the driving force for continuous research in combustion is to better understand, describe, and predict combustion processes to improve the efficiency of existing fuels and search for alternative fuels and renewable energy sources.

Combustion is basically a chemical reaction between substances, usually including oxygen, and is generally accompanied by the generation of heat and light in the form of a flame [2]. Many common combustion systems, such as the diesel engine or the open flame, take place under non-premixed conditions. That means the fuel and the oxidizer are initially separated and are mixed in the reaction zone [3].

This diploma thesis aims to characterize selected aspects of the combustion of hydrocarbon and alternative fuels in non-premixed flows. In particular, the investigated fuels are pure ethanol, three mixtures of ethanol with decane and pure decane. The work provides experimental and numerical results.

A counterflow burner is used for the experimental part and is performed at the University of California, San Diego. This device is employed in many laboratories for experimental work on flames because the stabilized flames have one-dimensional diffusion flame structures, which reduce the complexity [4]. The counterflow burner configuration is used here to investigate the critical conditions of autoignition and extinction of the five different fuels.

The simulations are used to predict the critical conditions of autoignition and extinction. Finally, the experimental results are analyzed and compared with these numerical results. This comparison is conducted to determine whether there is a discrepancy between the experimental and numerical results. If there is a difference, explanations and reasons are sought.

2 Fundamentals of Combustion

Theory and Theoretical Framework

To understand the experiments conducted and their results, it is beneficial to be familiar with some specific knowledge, terms, and parameters in combustion theory and chemistry. Therefore, this chapter is devoted to the fundamentals of combustion and the theoretical framework for the experiments.

2.1 Autoignition, Extinction, and Diffusion Flame

The main focus of this thesis is descriptions of the critical conditions of autoignition and extinction of selected fuels in non-premixed flows. Both autoignition and extinction mechanisms are important limiting phenomena in combustion theory [5] and of fundamental and practical importance.

In combustion processes in non-premixed flows, the fuel and the oxidizer are initially separated before burning. Mixing of the fuel and the oxidizer is achieved by diffusion and convection [6]. For this reason, the flames produced in autoignition experiments and the flames extinguished in extinction experiments are non-premixed flames, also referred to as diffusion flames, to study these combustion behaviors.

These flames are generated in the experiments with a counterflow burner. This counterflow burner configuration helps measure the critical conditions of extinction and autoignition in non-premixed flows of selected fluids.

Autoignition

Autoignition occurs when liquids or gases ignite spontaneously without an external source of ignition like a flame or spark and after reaching a certain temperature. This certain temperature is called autoignition temperature.

In this process, air can serve as an oxidizer for the autoignition in the normal atmosphere.

Probably the best-known use of the autoignition phenomena is in the cylinders of diesel engines, where the fuel ignites because of the increase in temperature during the compression stroke.

Extinction

The extinction of a flame at a liquid surface occurs when the characteristic residence time is insufficient for chemical reactions to take place. This can be attained when the flow rate of the oxidizer is increased above certain values. This means that the residence time is much shorter than the chemical time, and as a consequence, chemical reactions cannot proceed fast enough to maintain a sufficient pool of reactive species against the flow of incoming reactants. [7]

The extinguishing condition can be characterized by the flow rates of the oxidizer that lead to flame extinction. However, such a parameter is not a specified property of the investigated fuels but a characteristic of certain experimental devices. A more basic parameter is called strain rate, which is the reciprocal of the characteristic residence time and allows comparisons between different laboratories with different experimental setups. The strain rate is the oxidant-side velocity gradient in the inviscid flow upstream of the flame and is discussed in Chapter 2.3. [7]

Diffusion Flame

The diffusion flame is a small section of the vast field of combustion theory. As mentioned above, diffusion flames are defined as any flame in which the fuel and the oxidizer are initially separated to the reaction zone. Therefore, diffusion flames are also known as non-premixed flames. Most practical systems lead to this kind of flame [6]. Common examples for diffusion combustion are met in open flames, diesel engines, gas turbine combustion chambers, and furnaces [3].

The other basic type of flames is premixed flames, where the fuel and the oxidizer are mixed before the reaction. Typical examples for premixed flames are the Bunsen burner flame and the flames in most spark-ignited engines [3]. In the present work, premixed flames are not considered.

Apart from when the fuel and the oxidizer get mixed, another difference is that diffusion flames produce larger amounts of pollution (particularly soot) and are more difficult to control than premixed flames [8].

As mentioned at the beginning of this chapter, these diffusion flames are generated with a counterflow burner. This device is often used in laboratories for experimental work on flames because these generated flames represent one-dimension diffusion flame structures which reduce the complexity [4].

Essentially, the counterflow burner consists of two main parts: an upper part for the oxidizer and a lower part for the fuel. Figure 1 shows a simple illustration of a counterflow burner. There are several configurations of counterflow burners. The counterflow burner configurations used in the experiments of this thesis are discussed in detail in Chapter 3.1.

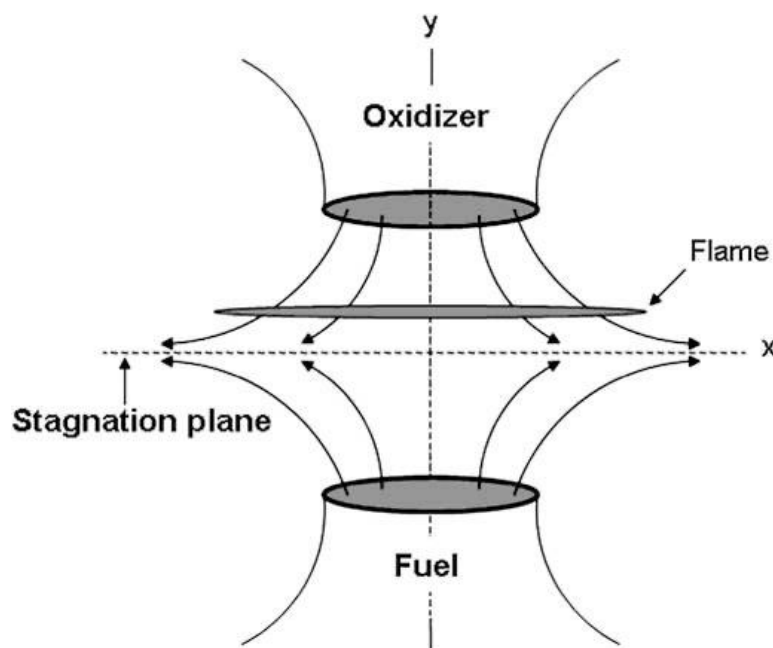


Figure 1: Schematic illustration of a diffusion flame generated by a counterflow burner [9]

One stream leaves the oxidizer duct, and the other stream leaves the fuel duct, as illustrated in Figure 1. Both the oxidizer stream and the fuel stream are assumed to be steady, laminar, and axisymmetric. These two uniform flows collide against each other. This creates a stagnation plane. Due to autoignition or manually ignition events, a flame occurs above the stagnation plane. This counterflow, axisymmetric laminar diffusion flame is stabilized in the boundary layer around the stagnation plane of the oxidizer and fuel stream [9].

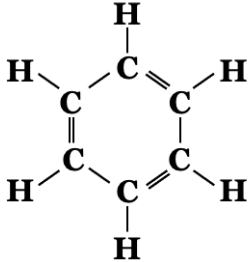
2.2 General Information on Hydrocarbons

As mentioned in the previous chapter, the experiments of this thesis serve to study the combustion of selected fuels. Essentially, these selected fuels are hydrocarbons and, in some cases, alternative fuels. Specifically, these selected fuels are ethanol and decane. Ethanol and decane are examined in various mixing ratios, see Table 4 in Chapter 3 for the exact mixtures.

Hydrocarbons are composed only of the elements carbon and hydrogen. This compound of carbons and hydrogens is one of the most significant classes of organic chemical compounds. Thereby, the carbon atoms join together to form the framework of the compound. The hydrogen atoms are attached to these carbon atoms in many different configurations. [10]

Depending on their sources and properties, there are two main groups of hydrocarbons: aliphatic and aromatic (see Table 1). The aliphatic group is divided into three subgroups according to the types of bonds between the carbons: alkanes (carbon-carbon single bonds), alkenes (carbon-carbon double bond), and alkynes (carbon-carbon triple bond). The focus of this thesis is on the group of alkanes. The aromatic compounds are characterized by special stability. If the aromatic compound contains a benzene ring as a structural unit, it is classified as a benzenoid aromatic compound. Without a benzene ring but meeting the criterion of special stability, it is a non-benzenoid aromatic compound. [10]

Table 1: Structures of representative hydrocarbons

Aliphatic Hydrocarbons			Aromatic Hydrocarbons
Alkane	Alkene	Alkyne	
$\begin{array}{c} \text{H} \quad \text{H} \\ \quad \\ \text{H}-\text{C}-\text{C}-\text{H} \\ \quad \\ \text{H} \quad \text{H} \end{array}$	$\begin{array}{c} \text{H} \quad \quad \text{H} \\ \diagdown \quad / \\ \text{C}=\text{C} \\ / \quad \diagdown \\ \text{H} \quad \quad \text{H} \end{array}$	$\text{H}-\text{C}\equiv\text{C}-\text{H}$	

Hydrocarbons are the primary constituent of fossil fuels, namely coal, petroleum, natural gas, oil shales, and heavy oils. Because of this, fossil fuel recourses are often referred to

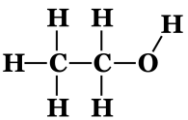
as hydrocarbon resources. The combustion of these fossil fuels produces heat. This heat serves as a source of energy. Today, fossil fuels have gained great technical importance and supply more than 80 percent of all the energy consumed by the industrially developed countries of the world. [11]

Fossil fuels are classified as non-renewable resources because they take millions of years to form and are consumed much faster than new ones are generated. Additionally, carbon dioxide is produced as one of the main by-products of fossil combustion. Carbon dioxide is a major contributing factor to human-induced global warming. Therefore, it makes sense to rely more on renewable energy sources. Alternative fuels are considered renewable sources. The U.S. Department of Energy defines alternative fuels as biofuel, ethanol, methanol, hydrogen, coal-derived liquid fuels, electricity, natural gas, propane gas, or synthetic transportation fuel [12]. It means that alternative fuels could consist of renewable and non-fossil hydrocarbons, such as ethanol.

2.2.1 Ethanol

Ethanol is a colorless and highly flammable liquid with a characteristic odor and is soluble in water infinitely. Its chemical formula is C_2H_6O . The main properties of ethanol are shown in Table 2.

Table 2: Properties of ethanol [13]

Chemical and Skeletal Formula	Molecular Weight	Density at 20 °C	Melting Point	Boiling Point
C_2H_6O 	46.07 g/mol	0.7893 g/cm ³	-114.1 °C	+78.2 °C

Ethanol is a simple alcohol. It derives from ethane (C_2H_6), in which a hydrogen atom has been formally replaced by a functional hydroxy group (-OH). Ethane is an aliphatic hydrocarbon depending on the group of alkanes.

The chemical compound alcohol is characterized by one or more functional hydroxy groups (-OH) attached to a carbon atom of a hydrocarbon chain [14].

Apart from being one of the most common alternative fuels, ethanol is also well-known as the type of alcohol people drink and use for disinfection.

Today, ethanol is produced mainly by microbial fermentation of sugars and starches from food crops like sugar cane and corn. However, growing food crops for ethanol production has a limited potential: competition from the food industry, limited agricultural land for crop growth, and high energy input requirements for agricultural chemicals and harvesting. [15]

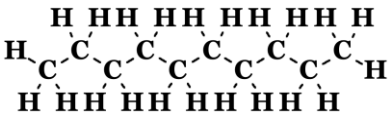
Consequently, this does not mean that using renewable resources such as sugar cane and corn for alternative fuels is particularly environmentally friendly.

To exploit the potential of biofuel ethanol as a suitable alternative fuel, lignocellulosic biomass must be considered. Lignocellulosic biomass is a plant-based material that is not used for the food industry and mainly includes agricultural residues and other wastes. Additionally, lignocellulosic biomass needs lower agricultural chemical requirements and lower energy requirements. Despite these advantages, the lignocellulosic feedstock is not yet economical for large-scale production because conversion to ethanol offset some of the possible energy savings. [15]

2.2.2 Decane

Like ethanol, decane is a colorless and readily combustible liquid with a characteristic odor. In comparison to ethanol, it does not dissolve in water. Its chemical formula is $C_{10}H_{22}$. 75 structural isomers are possible for decane. However, the term decane refers to the normal-decane with the skeletal formula $CH_3(CH_2)_8CH_3$, as delineates below in Table 3. Additionally, Table 3 shows some other characteristics of decane.

Table 3: Properties of decane [16]

Chemical and Skeletal Formula	Molecular Weight	Density at 25 °C	Melting Point	Boiling Point
$C_{10}H_{22}$ 	142.28 g/mol	0.7255 g/cm ³	-29.7 °C	+174.1 °C

Decane is an aliphatic hydrocarbon belonging to the group of alkanes.

It is an important commercial chemical with various applications: component of engine fuel, production of other chemicals, solvent, and jet-fuel research chemical [16].

The chemical compound decane is a saturated hydrocarbon. These saturated hydrocarbons are mostly obtained from the two natural sources of natural gas and petroleum, either by isolation such as distillation or by suitable conversion reactions [16].

2.3 Strain Rate, Damköhler Number, and S-shaped Curve

The theoretical framework for the experiments is based on the critical value of the Damköhler number, which is defined as the ratio of a characteristic flow time to a characteristic reaction time. The flow time is the reciprocal of the strain rate. The so-called S-shaped curve is a way to visualize the critical conditions of autoignition and extinction in non-premixed flows depends on the Damköhler number.

Strain Rate

To accurately characterize the flow field and quantify the velocity of the oxidizer and fuel flow of the counterflow burner, the parameter of the so-called strain rate is used. The two mentioned flows have already been shown above in Figure 1. The strain rate of the oxidizer stream is significant for the experiments. Thus, when this work refers only to a strain rate, it always means the oxidizer strain rate.

Derived by Seshadri et al., the strain rate is generally defined as the normal gradient of the normal component of the flow velocity [17] [18]. The strain rate is the reciprocal of a

characteristic flow time in the flow field of a counterflow flame [4]. Equation (2-1) represents the strain rate a_2 of the oxidizer duct at the stagnation plane:

$$a_2 = \frac{2|V_2|}{L} \left(1 + \frac{|V_1| \sqrt{\rho_1}}{|V_2| \sqrt{\rho_2}}\right). \quad (2-1)$$

Index 1 indicates the fuel boundary, and index 2 the oxidizer boundary.

The fuel boundary lies between the outer inviscid region of the fuel stream and the inner viscous boundary layer. The oxidizer boundary lies between the outer inviscid region of the oxidizer stream and the inner viscous boundary layer. [17]

V_1 and V_2 in Equation (2-1) represent the normal components of the flow velocities for the fuel and oxidizer stream at the boundaries in meters per second. The two boundaries are separated by the separation distance L in meters. Further, ρ_1 and ρ_2 denote the densities of the fuel and oxidizer stream at the boundaries in kilograms per cubic meter.

In the experiments performed in this thesis, the flow velocity of the fuel stream V_1 is small because the liquid fuels under investigation are in a fuel cup in the lower part of the counterflow burner, see Chapter 3.1.1 for detailed information about the counterflow burner. Therefore, Equation (2-1) simplifies to

$$V_2 = \frac{a_2 L}{2}. \quad (2-2)$$

This Equation (2-2) makes it possible to calculate the velocity of the oxidizer stream for a given oxidizer strain rate. That also means the higher is the strain rate of the oxidizer stream, the higher is the velocity of the oxidizer stream.

Damköhler Number

As mentioned at the beginning of Chapter 2.1, diffusion flames in a counterflow burner have two limits: autoignition and extinction.

In computational models, the causes of these two limiting phenomena can be obtained using the Damköhler number. The Damköhler number is a characteristic quantity for diffusion flames and a dimensionless ratio. There is a separate Damköhler number for extinction Da_E and for ignition Da_I . In general, the Damköhler number Da is defined as

$$Da = \frac{t_D}{t_R} \quad (2-3)$$

where t_D represents the characteristic diffusion time and t_R is the characteristic reaction time at a boundary temperature [19]. The diffusion time t_D depends on the flow field, which is imposed by the strain rate. The reaction time t_R is specified by the concentration of the reactants, the temperature before the reaction, and pressure. The reaction time t_R indicates the reactivity of the reactants. This means slow chemical reactions have low Damköhler numbers. High Damköhler numbers, on the other hand, indicate fast chemical reactions.

S-shaped Curve

The Damköhler number is also often used to visualize the concept of the two combustion limits autoignition and extinction. Thereby, the maximum reaction temperature T_{\max} in the reaction flow field or the burning rate is plotted as a function of the Damköhler number Da . This results in a regular, folded S-shaped curve, as first studied by Fendell [20] and Liñán [19]. The folded S-shaped curve consists of three possible solution branches concerning the counterflow burner configuration (see Figure 2):

- Lower branch (nonburning region) represents the maximum temperature of the reactants before the ignition event. This temperature coincides with the oxidizer temperature.
- Middle branch (unstable) cannot be studied experimentally [4].
- Upper branch (burning flame region) indicates the maximum temperature of the burning flame at different strain rates.

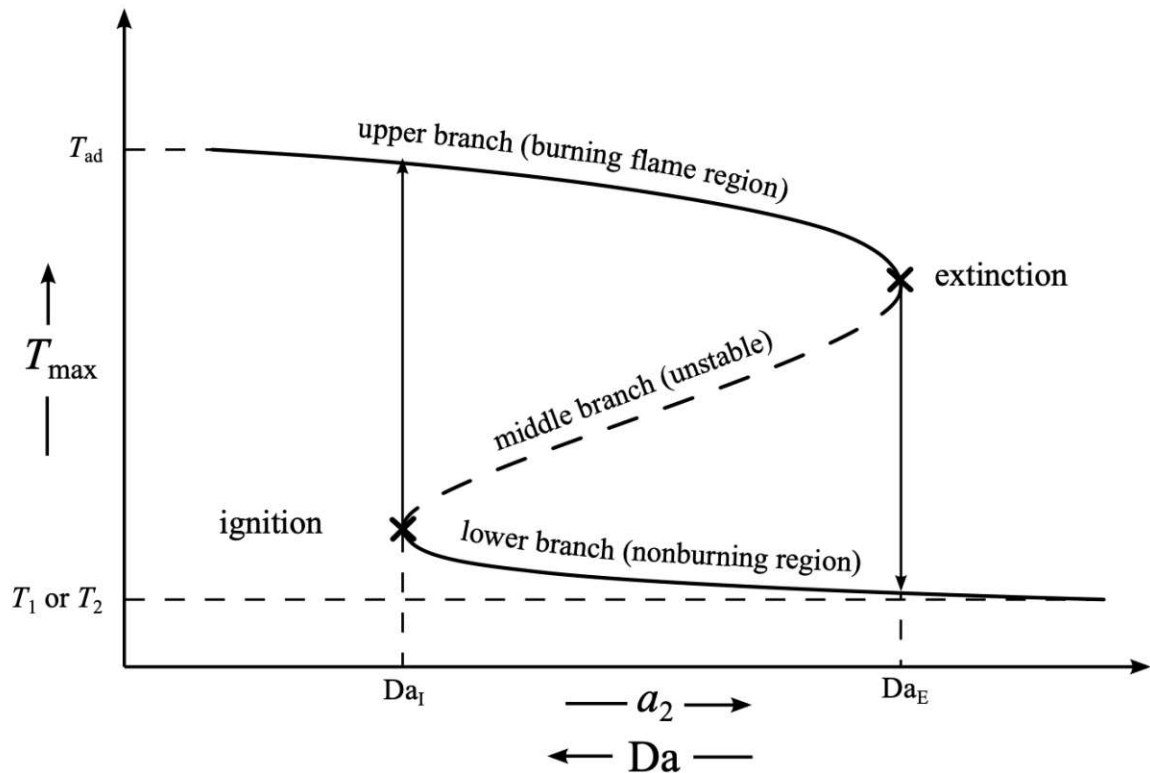


Figure 2: S-shaped curve – maximum temperature in the reaction zone as a function of the Damköhler number [4]

In the lower branch, the two opposite streams of the counterflow burner can be considered frozen since the chemical reactions are negligible. The maximum temperature in this flow field is equal to the higher temperature of the two streams – to the temperature at the fuel boundary T_1 or the oxidizer boundary T_2 .

By decreasing the strain rate in the lower branch, the Damköhler number increases because of a rise in the diffusion time t_D of the reactants. Simultaneously, the temperature rises to a critical point, the Damköhler number at ignition Da_I , where the mixture ignites. The maximum adiabatic flame temperature T_{ad} of this ignition is plotted along the upper branch of the S-shaped curve. Autoignition events like this can also be achieved by increasing the temperature at a constant strain rate.

By increasing the strain rate in the upper branch, the diffusion time t_D decreases. At the same time, the maximum temperature of the flame falls. At a certain strain rate and the Damköhler number at extinction Da_E , the flame is no longer stable and extinguishes. After the extinction of the flame, the maximum temperature of the flows drops immediately to the lower branch.

3 Experimental Setup and Procedure

The experimental investigation is concerned with the measurement of critical conditions of autoignition and extinction for several liquid fuels with air as the oxidizer. The fuels tested are ethanol and mixtures of ethanol with decane and pure decane, as shown in Table 4.

Table 4: Overview of investigated fuels

	1. Investigated Fuel	2. Investigated Fuel	3. Investigated Fuel	4. Investigated Fuel	5. Investigated Fuel
Ethanol [vol%]	100	80	50	20	
Decane [vol%]		20	50	80	100

The autoignition and extinction experiments are carried out at atmospheric pressure employing the counterflow burner constructed at the University of California, San Diego. The counterflow burner is well-known in combustion research to investigate laminar flames and has been used since the early 1960s [21]. The experimental setup and the procedure are described in the following two Chapters 3.1 and 3.2.

3.1 Experimental Setup for Autoignition and Extinction

A schematic illustration of the experimental setup is shown in Figure 3. The central component of the setup is the counterflow burner. The counterflow burner comprises two parts: an upper part (1A in Figure 3) with a duct for the oxidizer stream that faces a lower part (1B in Figure 3) with an axisymmetric fuel cup for the liquid fuel. A syringe pump (2 in Figure 3) is used to supply the fuel cup of the counterflow burner with the investigated fuels. A camera is installed next to the fuel to provide visual feedback for controlling the liquid level (3 in Figure 3). At the end of the oxidizer duct, a thermocouple

(4 in Figure 3), which is connected to a computer with control software (5 in Figure 3), is installed to monitor the temperature of the oxidizer stream. The needed gas for the counterflow burner comes from cylinders and the in-house gas system (6 in Figure 3). The flow of these gases is controlled by mass flow controllers (7 in Figure 3). The mass flow controllers and the pump are monitored and adjusted by a computer with control software (5 in Figure 3). The exhaust gases produced are discharged through an exhaust system (8 in Figure 3). All these components of the experimental setup are explained in more detail in Chapters 3.1.1 to 3.1.6.

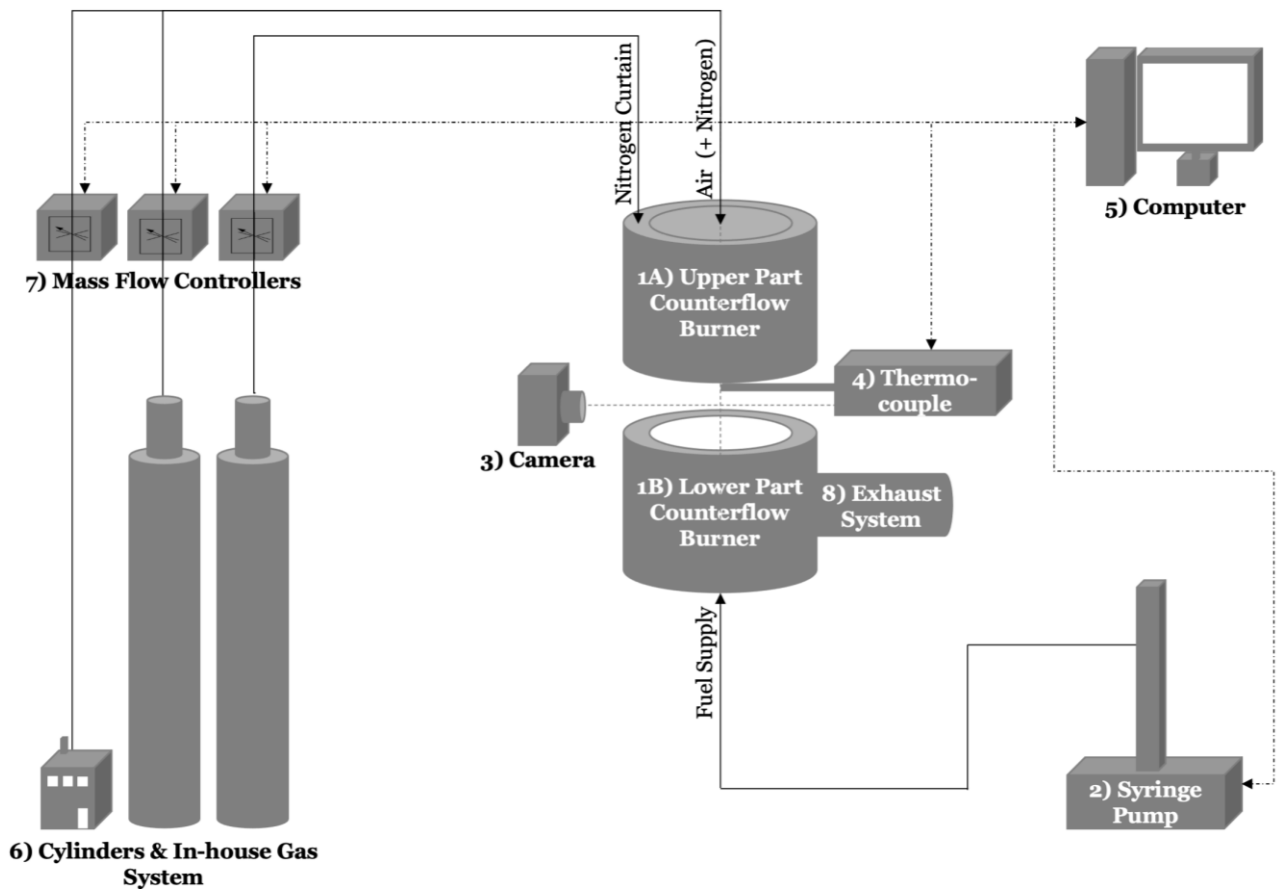


Figure 3: Schematic illustration of the entire experimental setup for the autoignition and extinction experiments

3.1.1 Counterflow Burner

As mentioned above, the counterflow burner is the main part of the experimental setup. It consists of two main parts: a lower part for the fuel and an upper part from which a mixture of air and nitrogen is injected into the mixing layer. Three adjustable pins connect these two parts. To investigate the autoignition and extinction of the five fuels described in Table 4, two different configurations are required for the upper part of the counterflow

burner, one for autoignition experiments and the other for extinction experiments. The lower part for the liquid fuels is identical for both configurations.

Autoignition Configuration of Counterflow Burner

Figure 4 shows the configuration for the counterflow burner for the autoignition experiments.

To achieve autoignition events, the temperature of the oxidizer stream needs to be increased gradually. To achieve this, a heating element is placed at the center of the upper part. It is surrounded by a machined quartz tube. The oxidizer stream also flows inside this quartz tube which represents the so-called oxidizer duct. The Starbar® heating element SER employed to heat the oxidizer stream is made of high-density reaction-bonded silicon carbide. It has an overall length of 268 millimeters and a diameter of 19 millimeters. Two electrical connections are made of flat braided aluminum straps at one end. These aluminum straps provide an easy connection to the power supply. For the experiment's power supply is used the variable transformer 3PN2210B from Staco Energy Products Company.

If an autoignition event occurs, the flame should be shielded from the environment. For this reason, a concentric nitrogen curtain encircles the reaction zone from the upper part of the burner. To extinguish the flame after the autoignition event, the flow rate of the nitrogen in the oxidizer stream is increased. The supply of nitrogen, as well as air, is described in Chapter 3.1.3.

Three fine screens are placed at the exit of the oxidizer duct to achieve plug flow conditions with high accuracy [4]. These screens are made of Inconel 600 mesh and are held by steel rings.

The entire upper part of the counterflow burner in autoignition configuration is isolated with flexible silica fiber sheets.

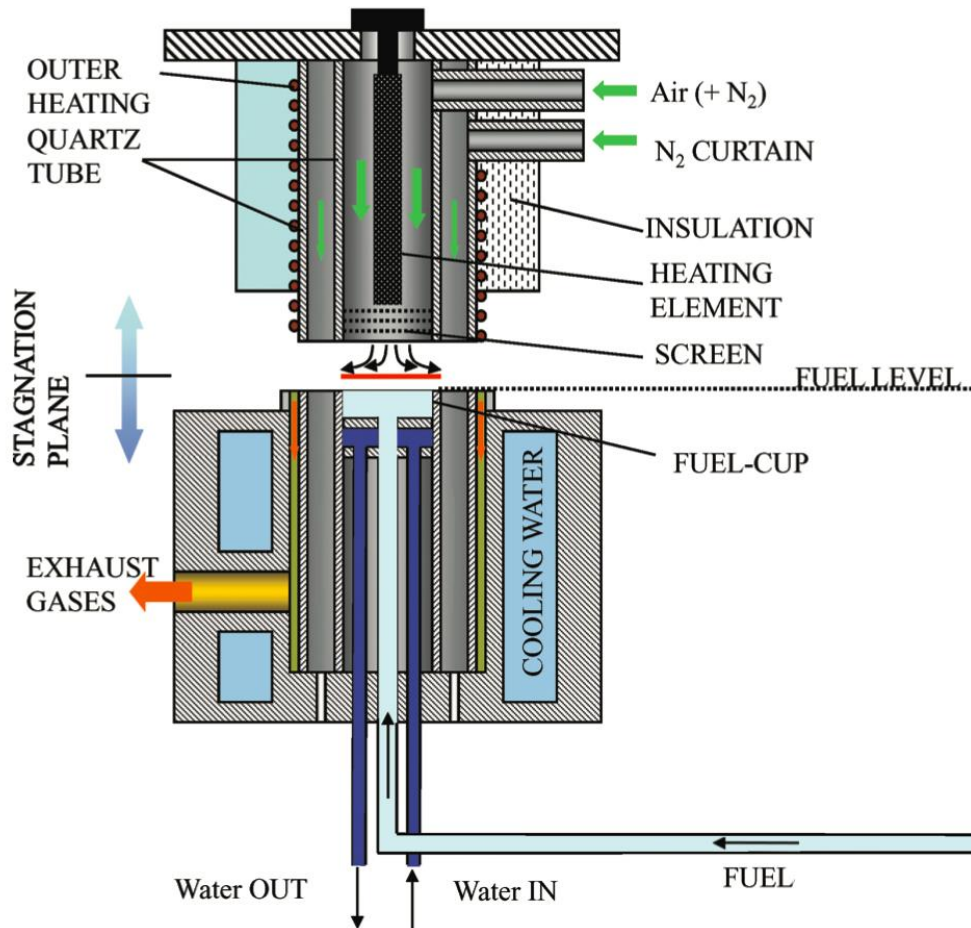


Figure 4: Schematic illustration of the autoignition configuration of the counterflow burner – figure slightly modified from [22]

The separation distance between the oxidizer duct outlet and the fuel cup is set to 0.012 meters for the experiments.

The fuel cup is in the middle of the lower part in Figure 4, and it has a depth of 10 millimeters and an inner diameter of 35 millimeters. The level of the fuel cup is visually monitored by an indicator needle (see Figure 5). The surface of the liquid is maintained at a position where the needle tip causes a small dimple on its surface. If the needle tip is visible, the level is too low. Otherwise, the level is too high when the dimple disappears.

The supply of the fuel cup is detailed described in Chapter 3.1.2.

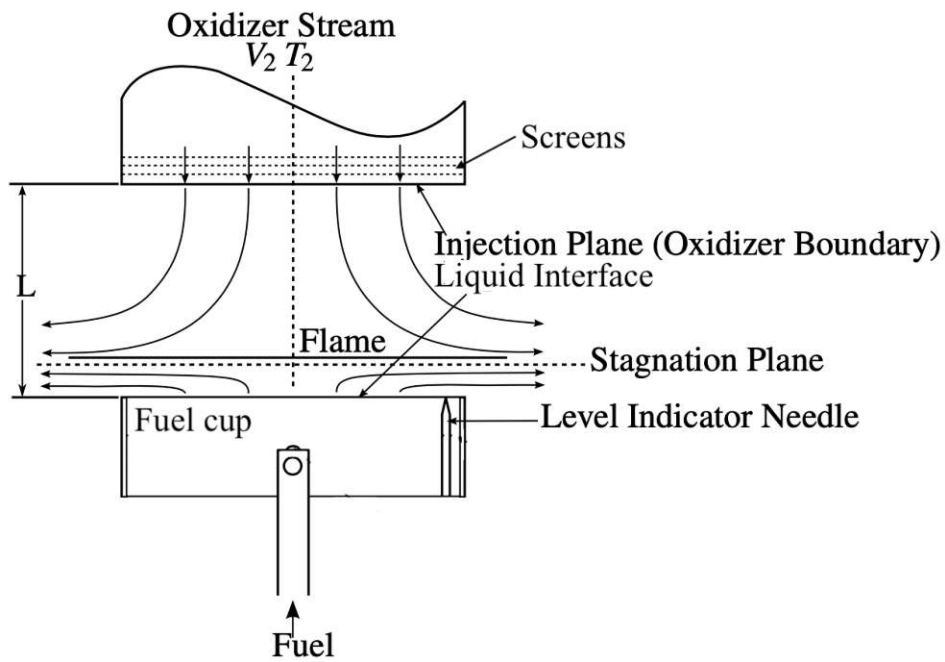


Figure 5: Schematic cutaway view of the counterflow configuration for autoignition experiments – figure slightly modified from [4]

Apart from the fuel cup, the lower part consists of a cooling water system used to protect the counterflow burner from damage and for the exhaust system. The exhaust system is explained in Chapter 3.1.6.

Figure 6 shows the used counterflow burner in autoignition configuration at the University of California, San Diego.

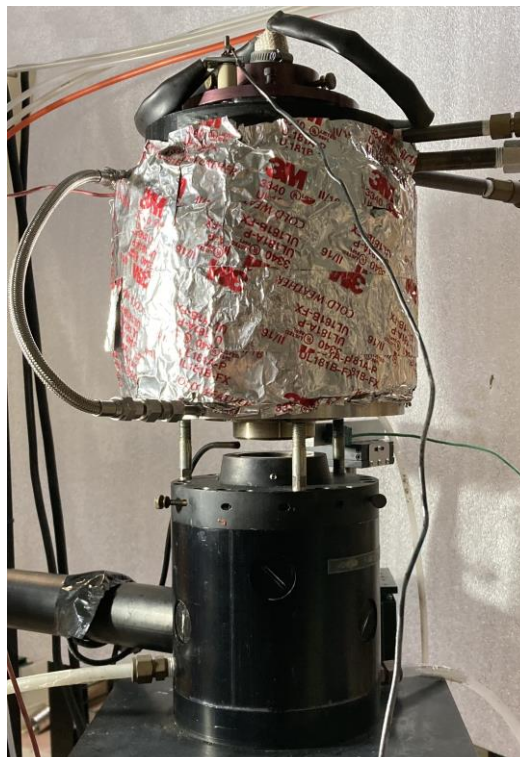


Figure 6: Counterflow burner in autoignition configuration at the University of California, San Diego

Extinction Configuration of Counterflow Burner

In the extinction experiments, the configuration of the lower part of the counterflow burner, including the liquid supply system and exhaust system, is the same as that for the autoignition experiments. Therefore, only the upper part of the counterflow burner in extinction configuration is discussed in the following section (see Figure 7).

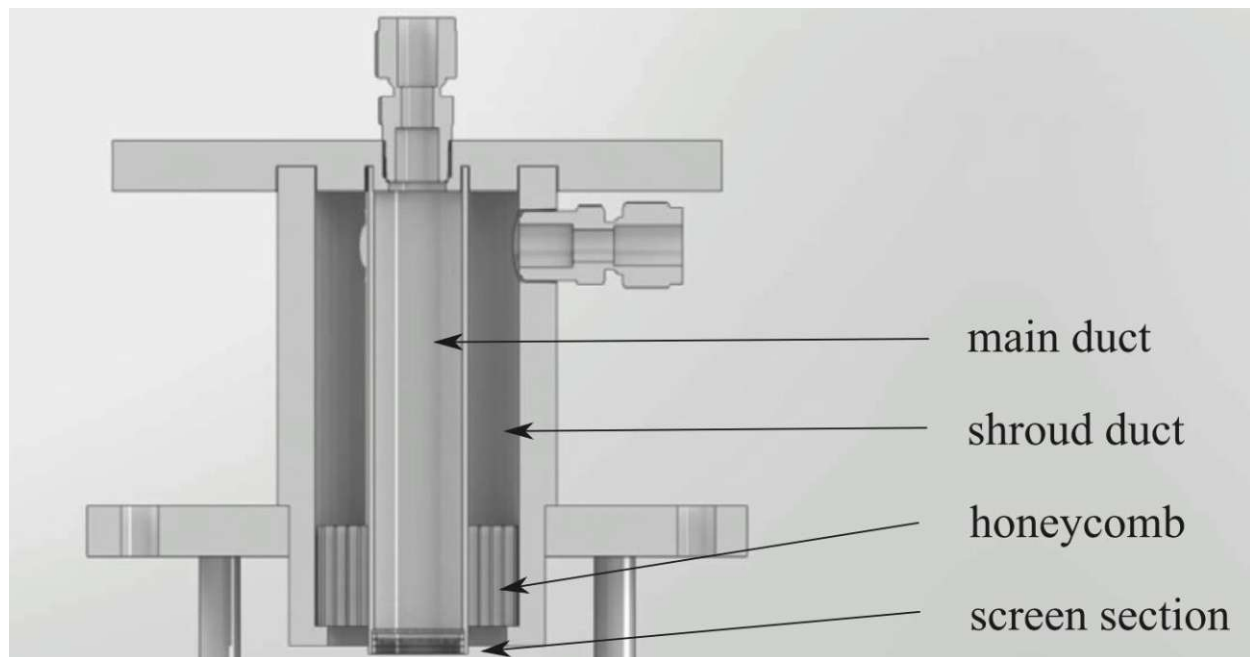


Figure 7: Schematic drawing of the upper part of the counterflow burner in extinction configuration – figure excerpt from [23]

Many design details of the upper part of the burner for extinction experiments are similar to those employed for the autoignition experiments: It again consists of an oxidizer duct that guides the oxidizer stream (air plus nitrogen) into the reaction zone. At the outlet of the oxidizer duct, there are again three screens made of Inconel 600 mesh, which are held by steel rings. These screens again help to assure plug flow conditions [4]. The oxidizer duct is again surrounded by a curtain duct through which the nitrogen curtain is passed. The nitrogen curtain again shields the reaction zone from the environment. In the extinction experiments, the distance between the upper and lower part is again set to 0.012 meters.

Despite these similarities, there are some key differences between the two upper parts in these two configurations: The extinction configuration does not have a heating element. Additionally, a ceramic honeycomb ring is inserted close to the outlet of the curtain duct to produce a uniform flow.

Figure 8 shows the used counterflow burner in autoignition configuration at the University of California, San Diego.



Figure 8: Counterflow burner in extinction configuration at the University of California, San Diego

3.1.2 Liquid Supply System

A Syringe pump supplies the lower part of the counterflow burner with the fuels tested by pumping them through the pipe connecting the fuel cup. In this setup, the Teledyne ISCO 500D syringe pump is used. This pump has a flow accuracy of 0.5 percent of setpoint. In the experiments conducted, the flow range is 0 to 15 milliliters per minute. To control and monitor the flow rate of the liquids, the pump has a serial interface (RS232/485) for communication with the control software, which is described in Chapter 3.1.5.

3.1.3 Gas Supply and Control System

As seen in Figure 3, air and nitrogen are required for the experiments. The high-pressured nitrogen is provided in cylinders. Pressurized air is used for the oxidizer stream. The air comes from the in-house air system.

For accurate flow control of the gases, Teledyne HFC-302 mass flow controllers are installed to automatically establish the flow rate of the gases according to the setting.

The range of these controllers is from 0 up to 100 standard liters per minute. The in-house air system, the nitrogen cylinder for the oxidizer, and for the curtain have their own mass flow controllers.

All three mass flow controllers are powered and controlled by two Teledyne PowerPod-400 Power Supply modules. These modules are communicating with the control software (see Chapter 3.1.5) via an interface (RS232).

3.1.4 Temperature Measurement

A thermocouple located at the oxidizer duct outlet measures the temperature of the oxidizer stream (see Figure 9).

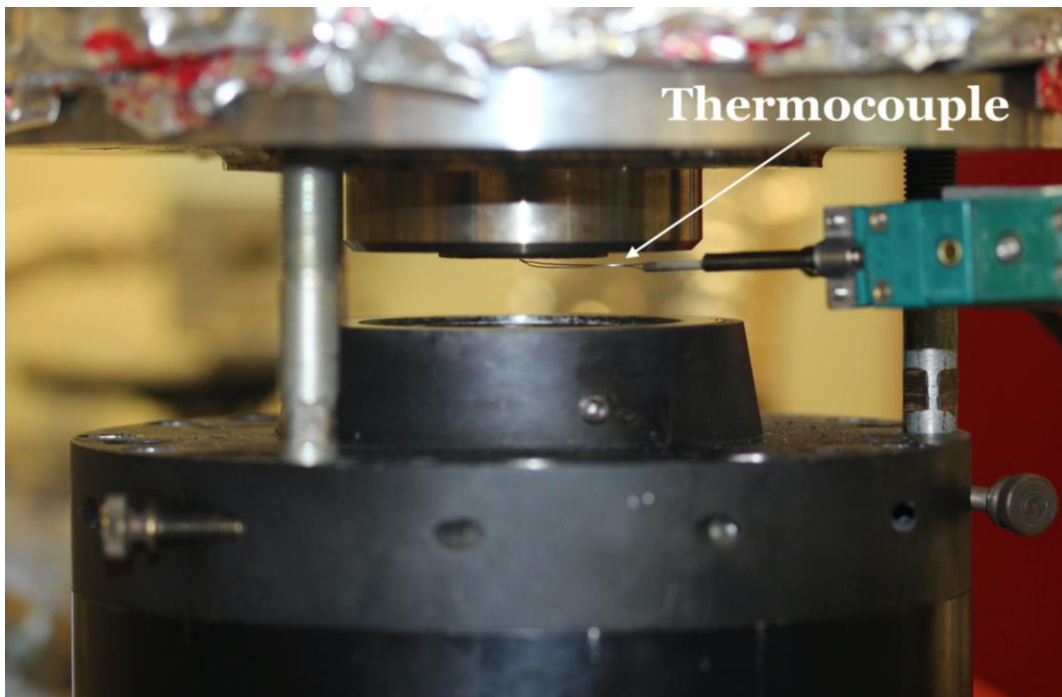


Figure 9: Type R thermocouple between the lower and upper part of the counterflow burner

Thermocouples are very common for temperature measurements, thanks to their robustness, low cost, and ease of installation [24].

They consist of two dissimilar metal wires joined together at two junctions. If a temperature difference exists between the junction of the two metals, a change of the voltage can be measured. The actual temperature can be determined from the current flow. [25]

Type R, Pt/13%Rh-Pt thermocouple with a wire diameter of 0.2 millimeters are used in the experiments. The influence of this thermocouple on the flow field is presumed to be small and is neglected.

However, using the thermocouple in high-temperature environments, the temperatures measured are influenced by radiative heat losses from the bead of the thermocouple. Therefore, a correction of the autoignition temperatures measured is necessary. This correction is described in detail in Chapter 4.1.

3.1.5 Control Software

Control software is required to control and monitor the entire experimental setup as heating system, liquid supply system, gas supply and control system, and temperature measurement as described above.

The used software is a graphical programming language by National Instruments called LabVIEW™ (Laboratory Virtual Instrument Engineering Workbench). This programming environment uses icons instead of lines of text to create applications and has proven itself in many scientific fields [26].

Figure 10 shows the LabVIEW™ user interface, also called front panel when an autoignition event occurs during the experiments. The most important areas of the front panel are marked and numbered there.

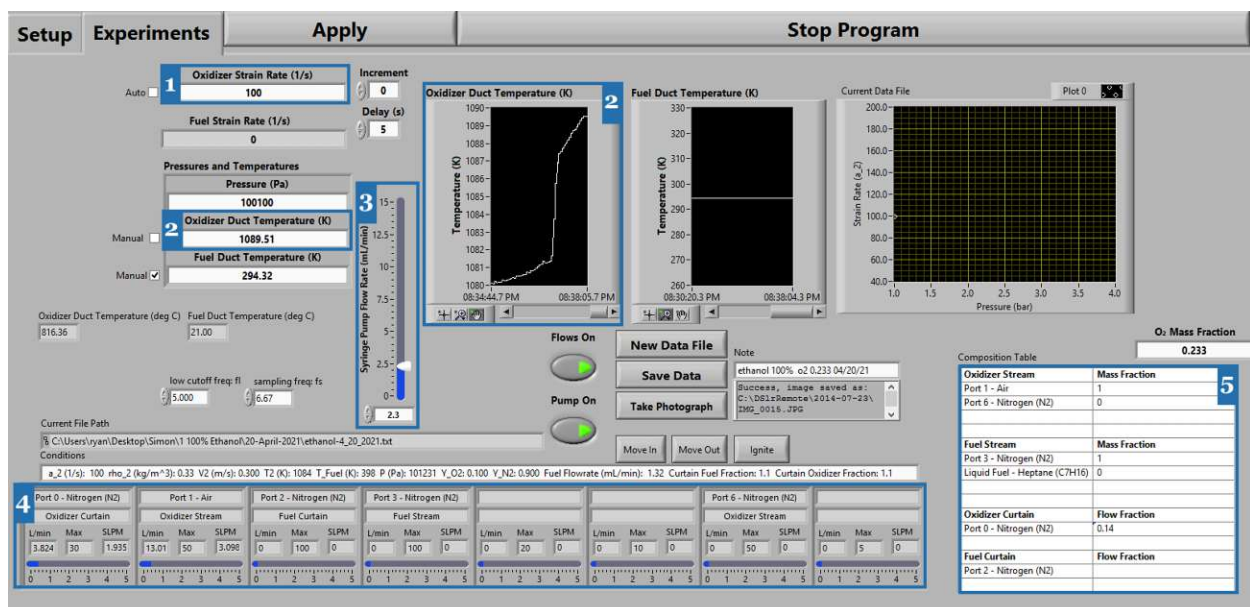


Figure 10: LabVIEW™ user interface during an autoignition event of 100 vol% ethanol at a strain rate of 100

1. Input of the oxidizer strain rate
2. Monitoring of the exact oxidizer duct temperature and the temperature profile of the oxidizer duct during the last 40 seconds
3. Adjustment of the syringe pump flow rate to supply liquid to the fuel cup by using the slider
4. Display of the oxidizer stream and the curtain stream in liters per minute and standard liters per minute
5. Controlling and setting of the mass fractions of the oxidizer stream and the curtain stream

3.1.6 Exhaust System

As shown in Figure 4, the counterflow burner is equipped with an exhaust system. This exhaust system is connected to the internal building extraction system. Products are removed from the reaction zone by a weak vacuum, and care is taken to ensure that it does not influence the experiment. The product gases are cooled and diluted using a fine water spray within the counterflow burner. The water spray also avoids further reactions in the exhaust system. Afterward, the main exhaust components of the combustion are sent to an aluminum pipe for gravity separation. It gets disassembled to the gaseous compounds, soot, and water. The solid compounds and water leave the separator to a draining system for water recovery. The building ventilation system removes the gaseous compounds.

3.2 Procedures for Autoignition and Extinction Experiments

Similar preparations of the setup must be made for the two types of experiments. However, the procedure for performing both types is completely different.

As already stated, all experiments are conducted at atmospheric pressure. Each experiment for each investigated fuel is carried out at least three times to obtain reliable results.

Autoignition Experiments

The autoignition experiments provide the autoignition temperatures of the five liquid fuels (see Table 4) at different values of strain rate with air as an oxidizer stream. This stream has a fixed oxygen mass fraction equal to 0.233 and a fixed nitrogen mass fraction equal to 0.767.

A few steps must be taken to prepare the experiment:

- The Inconel 600 mesh screens of the upper part are replaced before every second experiment.
- The separation distance between the oxidizer duct outlet and the fuel cup must be 0.012 meters.
- The Teledyne HFC-302 mass flow controllers are calibrated.
- The syringe pump is flushed and filled with the investigated fuel.
- The cooling water system, the nitrogen cylinders, and the in-house air system are turned on.
- The thermocouple is clean and as close as possible to the heating element in the area with the highest temperature.
- The oxygen mass fraction of the oxidizer stream is set to 0.233.
- The last preparation step is to ignite the liquid in the fuel cup with a blowtorch to ensure that all devices are working and the resulting test flame has the required shape.

The subsequent heat-up process is prolonged to avoid thermal stress or damage. When the first autoignition occurs, the temperature measured milliseconds before this event is noted as the autoignition temperature at the first set strain rate. The flame is extinguished by decreasing the oxygen mass fraction of the oxidizer stream from 0.233 to a value close to zero.

Once the temperature is below the previously measured autoignition temperature, the heating continues at the next strain rate and an oxygen mass fraction again of 0.233 until the next flame appears. This procedure is performed several times for eight different strain rates to verify the data points. During the entire experiment, the liquid level in the fuel cup must constantly be high enough to show a small dimple of indicator needle on the liquid surface.

Figure 11 shows the autoignition event of 100 vol% decane at a strain rate of 100.

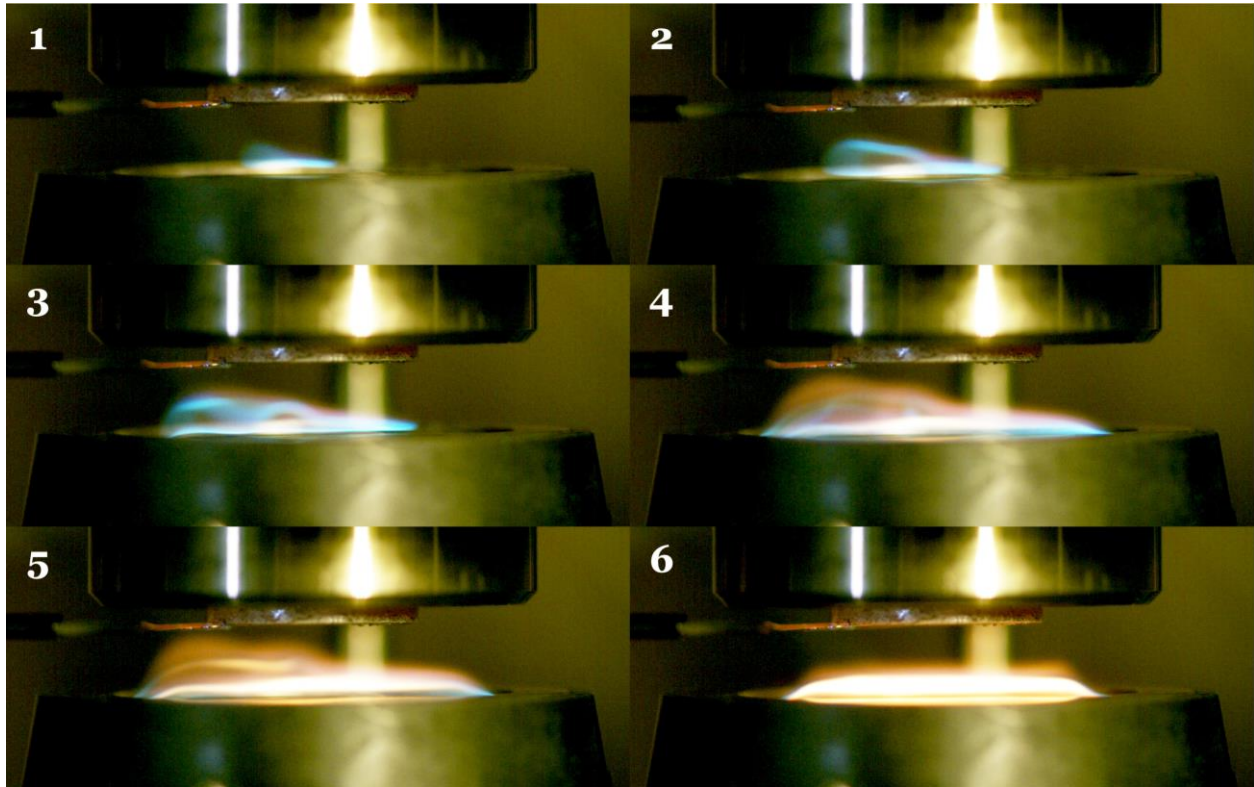


Figure 11: High-speed image of an autoignition event of 100 vol% decane at a strain rate of 100

Extinction Experiments

In these experiments, the extinction strain rates for the five fuels are measured at various oxygen mass fractions of the oxidizer stream. The value of the oxygen mass fraction varies in the range from 0.15 to 0.19.

For the most part, the same preparation for the extinction experiments must be done as before for the autoignition experiments. The main differences are that the thermocouple is not required for this kind of experiment, and the oxygen mass fraction of the oxidizer stream is set to 0.15.

Firstly, the investigated fuel is ignited with a blowtorch and a flame is established. Next, the strain rate is increased gradually. The value of the strain rate in one per second increases by 2 every 4 seconds. At a certain point, the strain rate is that high that the flame disappears. This procedure has been repeated a minimum of two times. However, with the difference that close to the previous extinction strain rate, the value of the strain rate increase in one per second is set to 1 every 3 seconds to obtain more precise results.

Then the oxygen mass fraction is increased by 0.1, and the procedure is repeated. Of importance for this experiment is the liquid level, which must always be at the desired position.

Figure 12 displays the extinction of 20 vol% ethanol and 80 vol% decane with an oxygen mass fraction of the oxidizer stream of 0.17.

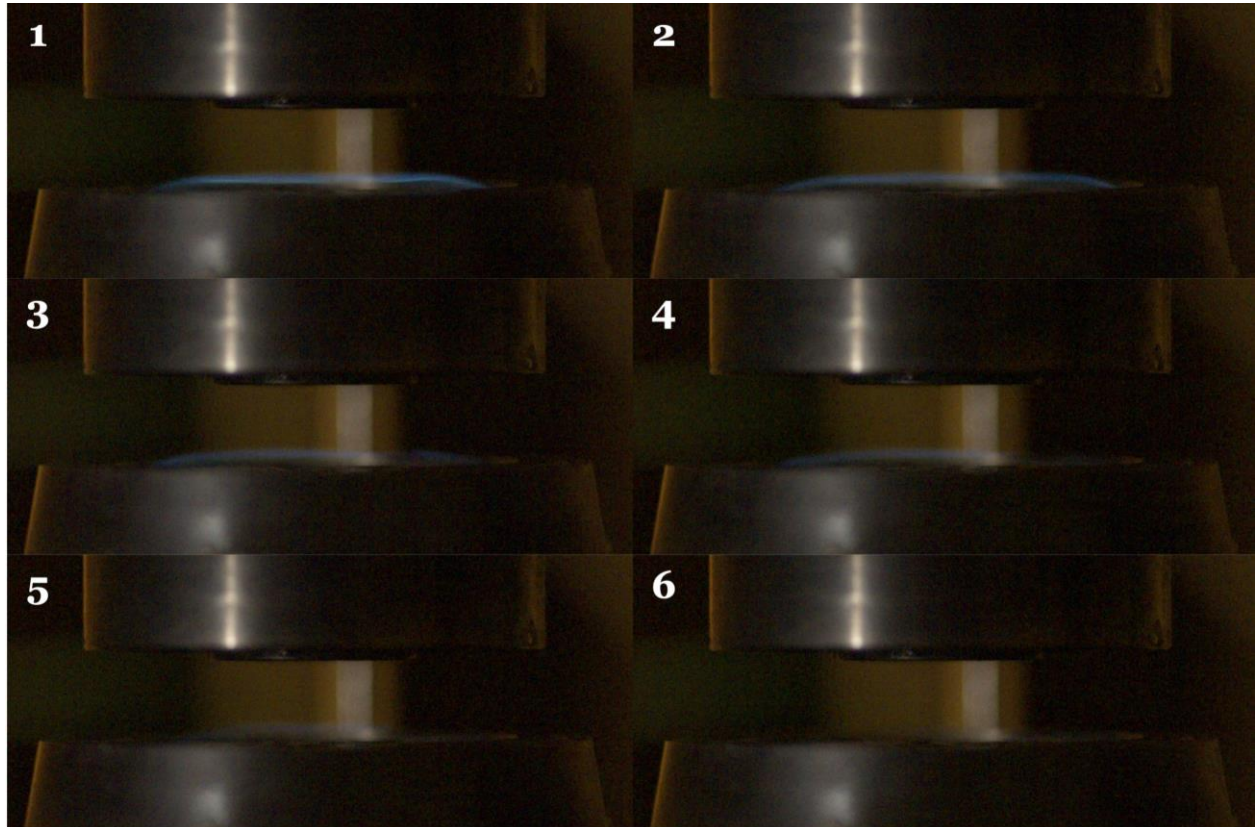


Figure 12: High-speed image of an extinction event of 20 vol% ethanol and 80 vol% decane at an oxygen mass fraction of 0.17

4 Experimental and Numerical Results

As described in Chapter 3.2, the main focus of the autoignition experiments is to measure the autoignition temperature at different values of strain rate with air as an oxidizer, while the emphasis of the extinction experiments is to evaluate the extinction strain rate at various oxygen mass fractions of the oxidizer stream.

The following subchapters are divided into two sections: The first section shows the autoignition results, and the second the extinction results.

4.1 Experimental Results

All the shown values of the conducted experiments are arithmetically averaged values. Each value is the average of at least three experimental runs. These values are displayed in detail in the Appendix.

Experimental Autoignition Results

As mentioned in Chapter 3.1.4, the temperatures measured using a thermocouple must be corrected to account for radiative heat losses from the bead. The measured temperature is not the actual temperature of the oxidizer stream. Rather it is the temperature of the thermocouple junction. For this reason, a correction of the initial experimental data is necessary. The raw data of the autoignition experiments without the correction are listed in the Appendix.

There are different approaches to correct the temperature. In this thesis, an approach most commonly employed in combustion literature [27] is taken to calculate the corrected temperatures. A newer method for computing the correction could be found in [28].

To estimate the radiant correction and the actual autoignition temperature, a convection-radiation energy balance is typically invoked (see Equation (4-1)) [27]

$$h (T_g - T_{tc}) = \varepsilon_{tc} \sigma (T_{tc}^4 - T_w^4) \quad (4-1)$$

where h describes the local convective heat transfer coefficient in watt per square meters kelvin, T_g the gas temperature, T_{tc} the thermocouple bead temperature, and T_w the temperature of the characteristic radiant surroundings, which are often dominated by a wall and is 295.15. All temperatures are given in kelvin. ε_{tc} stands for the dimensionless emissivity of the thermocouple, which is 0.22 ± 0.02 for Type R thermocouples [27]. This value was measured in the vicinity of 1400 kelvin by Grosshandler et al. in 1980. σ indicates the Stefan-Boltzmann constant in watt per square meters kelvin to the power of four with the value of $5.67 \cdot 10^{-8}$ [29].

In Equation (4-1), the convective coefficient h can be replaced by the definition of the dimensionless Nusselt number Nu which is

$$Nu = \frac{h d}{k} \quad (4-2)$$

with d for the thermocouple diameter in meters which is 0.2 meters, and k for the thermal conductivity of the gas in watt per meter kelvin with the value of 0.0759 at an air oxidizer stream temperature of 1200 kelvin [30]. Using this definition of the Nusselt number Nu in Equation (4-1) to replace convective coefficient h , the radiation correction for the gas temperature T_g can easily solve, as shown in Equation (4-3).

$$T_g = T_{tc} + \varepsilon_{tc} \sigma (T_{tc}^4 - T_w^4) \frac{d}{k Nu} \quad (4-3)$$

To solve Equation (4-3), the Nusselt number Nu for cylindric problems from Collis and Williams in 1959 is most commonly used. The Nusselt number for cylindric problems $Nu_{d,cyl}$ can be stated as seen in Equation (4-4) [27]

$$Nu_{d,cyl} = (0.24 + 0.56 Re^{0.45}) \left(\frac{T_a}{T_\infty} \right)^{1.7} \quad (4-4)$$

with T_a for the average temperature of the thermocouple and the oxidizer gas in kelvin and T_∞ for the temperature of the free stream of the oxidizer gas in kelvin. For simplicity, it is assumed that the last mathematical term in Equation (4-4) is one. That means T_a for

the average temperature of the thermocouple and the oxidizer gas and T_∞ for the temperature of the free stream of the oxidizer gas are almost equal. Equation (4-4) is obtained for a Reynolds number between 0.02 and 44 [27]. For the Reynolds number Re , another equation is needed. Equation (4-5) shows this formula.

$$Re = \frac{V_2 d}{\nu} \quad (4-5)$$

V_2 is the normal component of the flow velocities for the oxidizer stream at the boundary in meters per second and was previously determined with the help of the strain rate a_2 and the separation distance L in heated conditions of 0.0105 meters (see Equation (2-2)). d is again the thermocouple diameter in meters. ν is the viscosity of the oxidizer stream in square meters per second. Its value is 0.000158 at an assumed air oxidizer stream temperature of 1200 kelvin [30].

After determining the missing parameters, the gas temperature T_g can be defined with Equation (4-6). The gas temperature T_g describes the actual autoignition temperature.

$$T_g = T_{tc} + \varepsilon_{tc} \sigma (T_{tc}^4 - T_w^4) \frac{d}{k \left((0.24 + 0.56 \left(\frac{a_2 L}{2 \nu} \cdot d \right)^{0.45} \right) \left(\frac{T_a}{T_\infty} \right)^{17} \right)} \quad (4-6)$$

Table 5 summarizes all necessary variables at assumed air oxidizer stream temperature of 1200 kelvin for Equation (4-6) to determine the autoignition temperature T_g .

Table 5: Variables to calculate correction of thermocouple temperature at assumed air oxidizer stream temperature of 1200 kelvin [27] [29] [30]

T_{tc}	Temperature of thermocouple	Experiment dependent	K
ϵ_{tc}	Emissivity of Type R thermocouple	0.2	-
σ	Stefan-Boltzmann constant	$5.67 \cdot 10^{-8}$	W/m ² K ⁴
T_w	Temperature of surroundings	295.15	K
d	Diameter thermocouple	0.0002	m
k	Thermal conductivity	0.0759	W/mK
V_2	Flow velocity of oxidizer stream at boundary	Experiment dependent	m/s
ν	Viscosity of oxidizer stream	0.000158	m ² /s
a_2	Strain rate	Experiment dependent	1/s
L	separation distance in heated conditions	0.0105	m
T_a	Average temperature of thermocouple and oxidizer gas	Experiment dependent, neglected in simulation	K
T_∞	Temperature of free stream of oxidizer gas	Experiment dependent, neglected in simulation	K

Figure 13 displays the corrected results of the autoignition experiments of the five liquid fuels: 100 vol% ethanol, 80 vol% ethanol and 20 vol% decane, 50 vol% ethanol and 50 vol% decane, 20 vol% ethanol and 80 vol% decane, and finally 100 vol% decane.

Generally, the higher the oxidizer strain rate, the higher is the autoignition temperature, regardless of the fuel.

Figure 13 shows that at lower strain rates, the autoignition temperature increases with a larger decane share in the mixtures. In other words, pure ethanol or a mixture with high ethanol and small decane share is easier to ignite at strain rates below 200 than mixtures with small ethanol and high decane shares. Of all the investigated fuels, pure decane shows the lowest autoignition temperature at lower strain rates.

At higher strain rates (above 250), the phenomenon (pure ethanol or a mixture with high ethanol and small decane share is easier to ignite) can no longer be detected. At strain rates 400 and 450, the mixture 80 vol% ethanol and 20 vol% decane has the lowest autoignition temperature, whereas the mixture 50 vol% ethanol and 50 vol% decane has the highest one.

The exact values of this Figure 13, the values of the radiant correction, and the measured thermocouple temperature are attached in the Appendix.

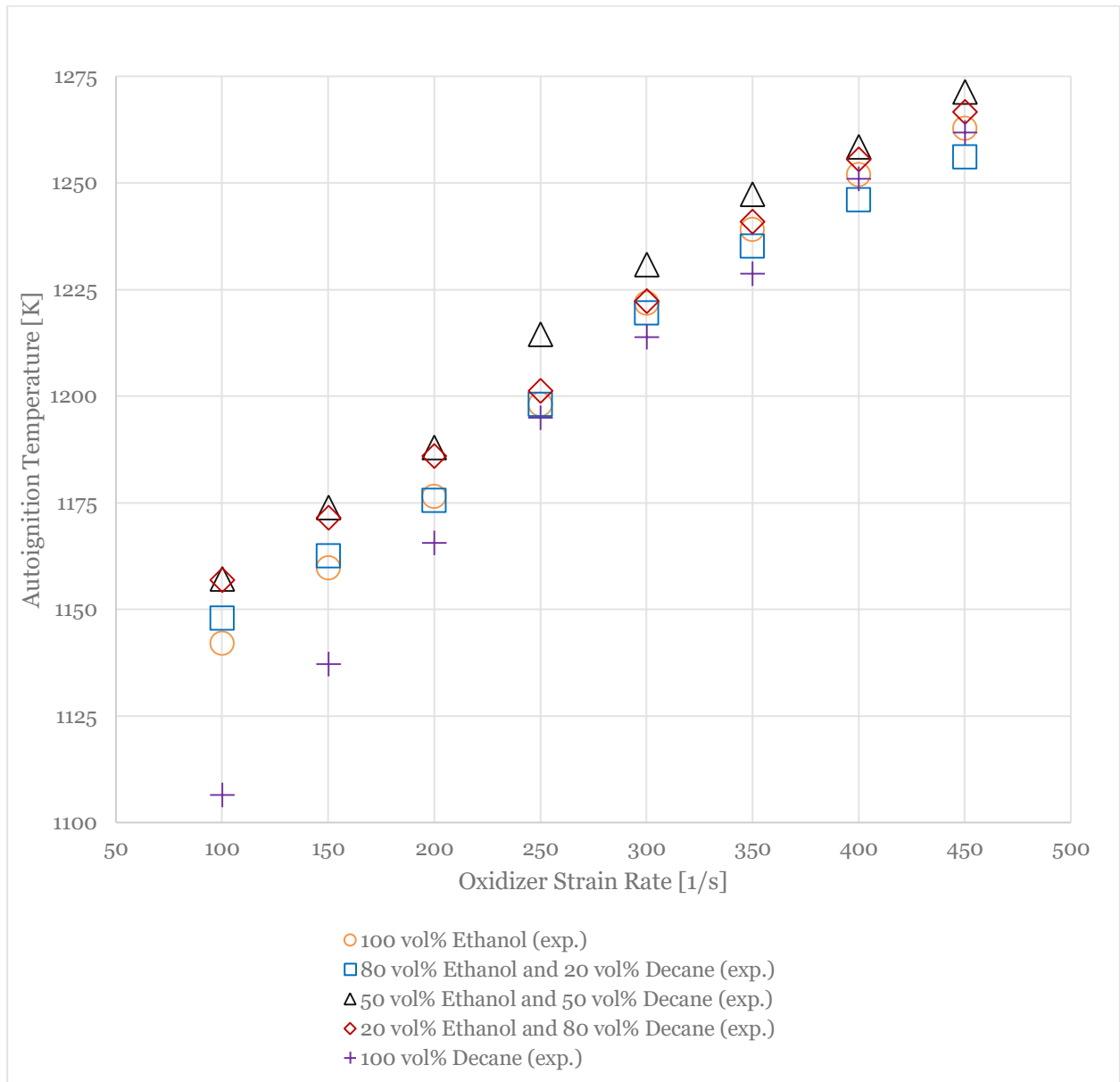


Figure 13: Corrected and averaged experimental autoignition temperatures of the five fuels as a function of the oxidizer strain rate

Experimental Extinction Results

In comparison to the experimental autoignition results, the extinction results can be directly used. Figure 14 displays the results of the five investigated fuels. In the following Figure 14, the extinction strain rate is plotted against the oxygen mass fraction of the oxidizer stream.

Generally, the higher the oxygen mass fraction of the oxidizer stream, the higher is the extinction strain rate, regardless of the fuel.

Additionally, there is a tendency that with higher ethanol content, the strain rate increases at a constant oxygen mass fraction of the oxidizer stream (especially at lower strain rates). Pure ethanol has for every value of the oxygen mass fraction the highest extinction strain rate. Whereas pure decane, except the oxygen mass fraction of 0.19, always shows the lowest extinction strain rates.

The strain rate of the mixture 80 vol% ethanol and 20 vol% decane shows only a small increase of the strain rate with a growing oxygen mass fraction. At an oxygen mass fraction of the oxidizer stream of 0.18, the extinction strain rate of this mixture falls below that of the other mixtures, which have a lower ethanol share. The strain rate of the mixture 80 vol% ethanol and 20 vol% decane even falls below the strain rate of pure decane at an oxygen mass fraction of 0.19.

The extinction strain rates of the mixture 50 vol% ethanol and 50 vol% decane and the mixture 20 vol% ethanol and 80 vol% decane are quite similar and do not indicate any special characteristics.

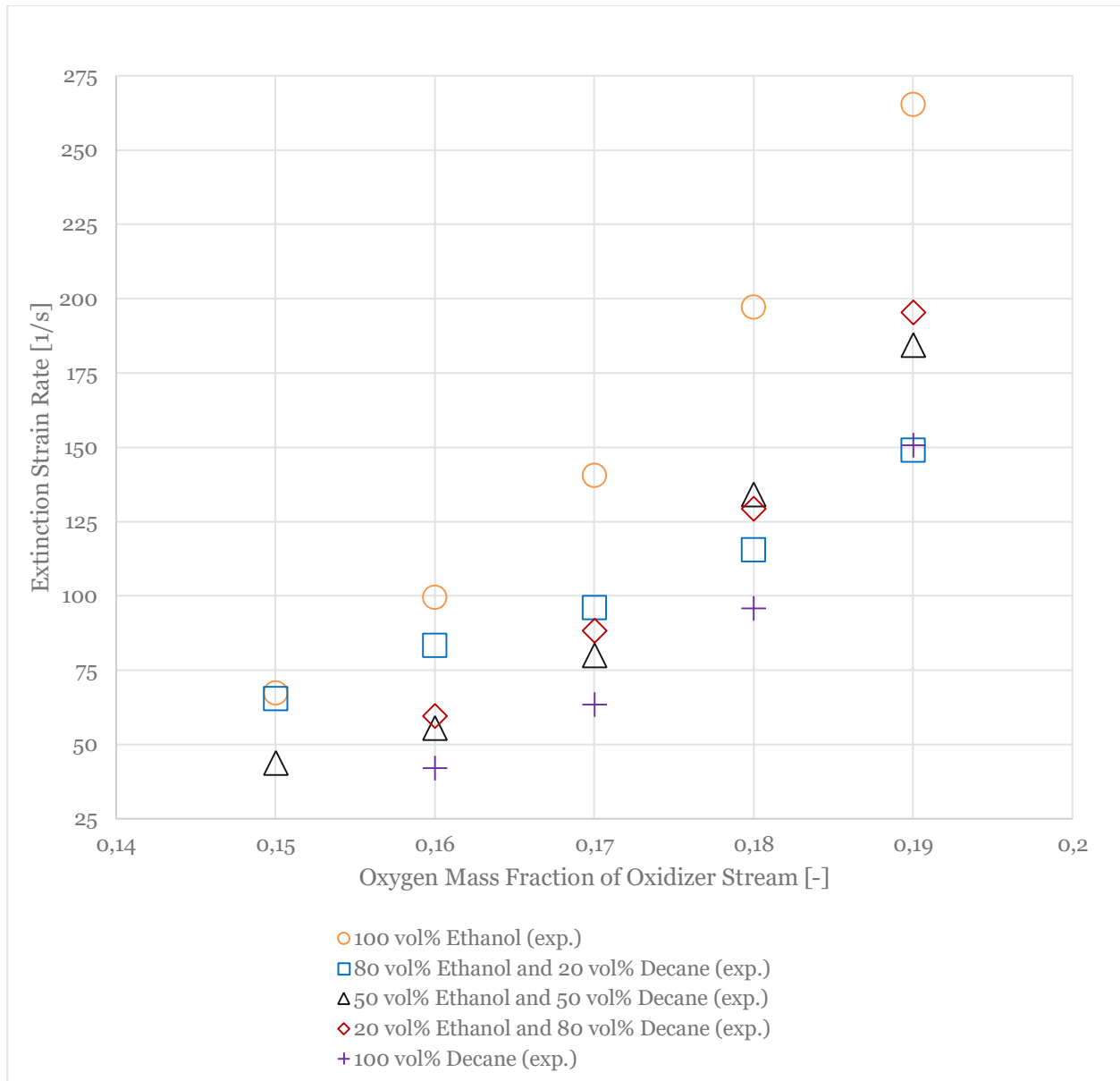


Figure 14: Averaged experimental extinction strain rates of the five fuels as a function of the oxygen mass fraction of the oxidizer stream

As presented above in Figure 14, there are no results for 100 vol% decane and the mixture 20 vol% ethanol and 80 vol% decane at an oxygen mass fraction of 0.15. This is because the counterflow burner in extinction configuration is not reliably usable at strain rates below 40. The strain rates of these two liquid fuels are too low, making it impossible to identify the experimental extinction strain rate at the lowest tested oxygen mass fraction.

4.2 Numerical Results

All presented numerical results in this thesis are determined by doing simulations with a general framework called OpenSMOKE++. The CRECK Modeling Group at Politecnico di Milano developed it for numerical simulations of reacting systems with detailed kinetic mechanisms, including thousands of chemical reactions and species. The OpenSMOKE++ framework is written in the general-purpose programming language C++. This framework can be extended and customized without modifying the core functions of the whole program. [31]

The CounterFlowDiffusionFlame1D solver and the kinetic mechanism C1-C16 HT+LT from the CRECK Modeling Lab of Politecnico di Milano are used for all the simulations. This mechanism (Version 2003, March 2020) includes high- and low-temperature chemistry, 492 species, and 17790 reactions [32].

To make the solver work, the velocity (by using the definition of the strain rate) and the compositions of the mixtures of the liquid fuels must be inserted. In the beginning, a steady-state simulation is performed to build the computational grid. The flow, energy, and species fields at initial conditions are calculated. Based on this steady-state simulation, a dynamic boundary condition is defined. The dynamic simulation is run until autoignition occurs by increasing the oxidizer temperature or until extinction occurs by increasing the strain rate.

The numerical computations of autoignition temperatures and the extinction strain rates were performed by Liang Ji of the University of California, San Diego.

Numerical Autoignition Results

Figure 15 presents the numerical results of the simulation for the autoignition of the five fuels. The calculated results for the autoignition temperature show for the pure fuels and the mixtures of ethanol and decane the same trend: By increasing the strain rate, every fuel is harder to ignite, and the autoignition happens at a higher temperature. The autoignition temperature is higher on a constant strain rate when the ethanol share is higher. That means pure ethanol has the highest autoignition temperature at every strain rate. Pure decane, on the other hand, is always the fuel that ignites most easily.

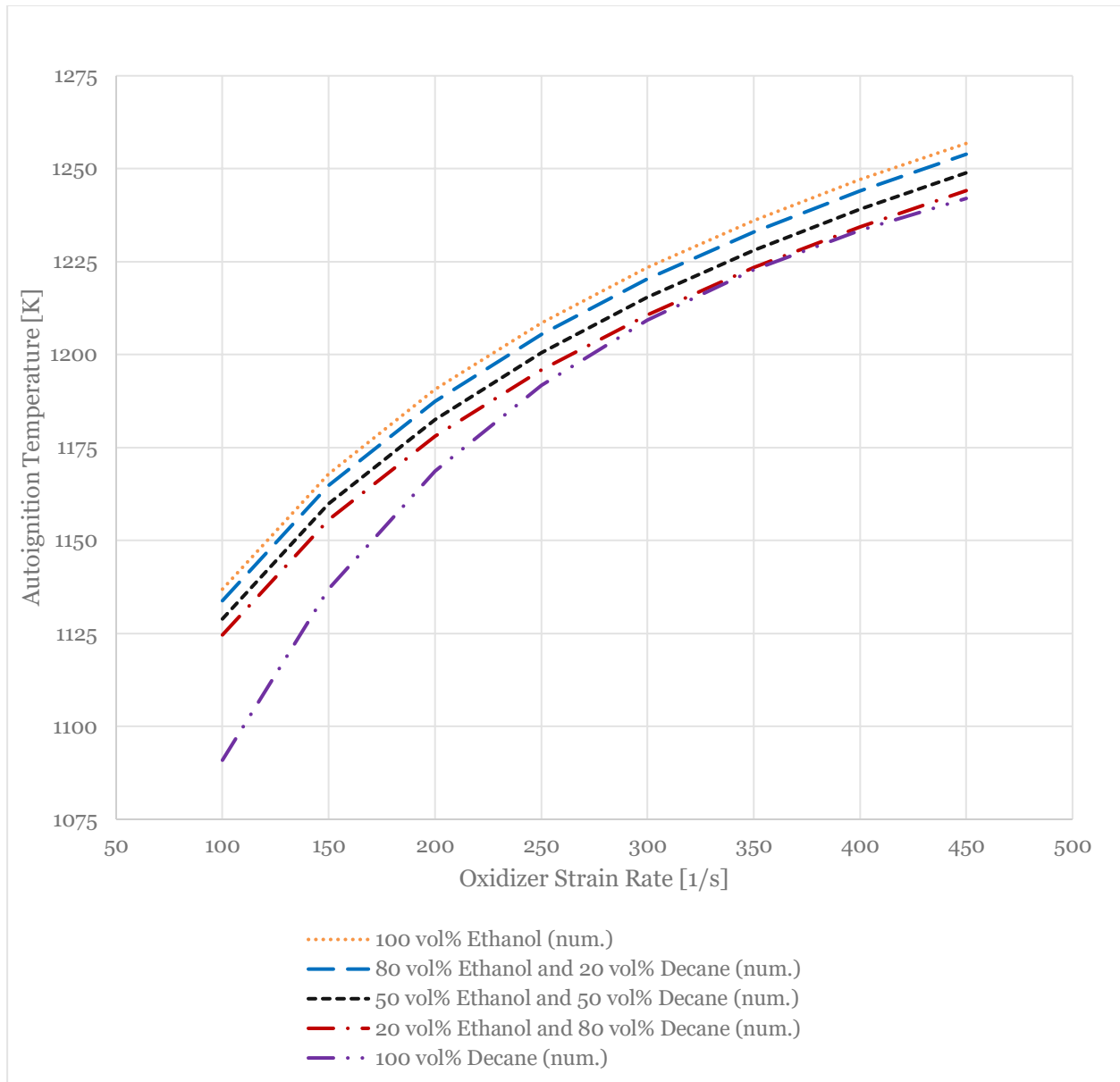


Figure 15: Numerical autoignition temperatures of the five fuels as a function of the oxidizer strain rate

Numerical Extinction Results

A problem occurs by performing the simulation with CounterFlowDiffusionFlame1D solver and the kinetic mechanism C1-C16 HT+LT to extinguish the flames of the five different fuels. It is impossible to ignite the fuels in the initial solution to build the computational grid in the simulation. The highest temperature in the simulation is the same as the boundary temperature. Consequently, that means no flame appears, and the extinction event cannot be simulated.

Even though all different parameters are changed for the simulation, it is not feasible to create an extinction event. For example, the flow speed was decreased, the oxygen mass

fraction of the oxidizer stream was increased, and the initial temperature of the simulation was changed.

After studying the solver and kinetic mechanism, it seems that some species like, for instance, ethanol in a liquid state, are not included in the kinetic mechanism, and the used kinetic mechanism only contains gaseous species. If this is the case, the different fuels cannot be ignited because there is no evaporation of the fuels.

Within the scope of this work, there is no possibility of performing the extinction simulations for 100 vol% ethanol, 80 vol% ethanol and 20 vol% decane, 50 vol% ethanol and 50 vol% decane, 20 vol% ethanol and 80 vol% decane, and finally 100 vol% decane.

Should the described solution actually represent the problem solution and the way to solve the issue, the existing kinetic mechanism must be extended by the liquid species, or a new kinetic mechanism must be developed. All these things could only be done by the CRECK Modeling Group at Politecnico di Milano.

4.3 Comparison and Discussion of Experimental and Numerical Results

In this chapter, the focus is on comparing and discussing the experimental and numerical results. Obvious deviations are pointed out in the figures. In addition, the following section explains and discusses why there may be differences in the results.

Comparison and Discussion of Autoignition Results

Figure 16 below shows that the experimental and numerical results do not match precisely.

As presented in Chapter 4.1, the experiments have shown that the autoignition temperature increases at particularly lower strain rates with a higher decane share in the mixtures. From the strain rate values of 250 to the maximum of 450, the mixture of 50 vol% ethanol and 50 vol% decane has the highest autoignition temperature.

On the other hand, the numerical simulation provides the result, as already mentioned in Chapter 4.2, that the higher the ethanol shares at a constant strain rate, the higher the autoignition temperature. This means pure decane always has the lowest numerical autoignition temperature.

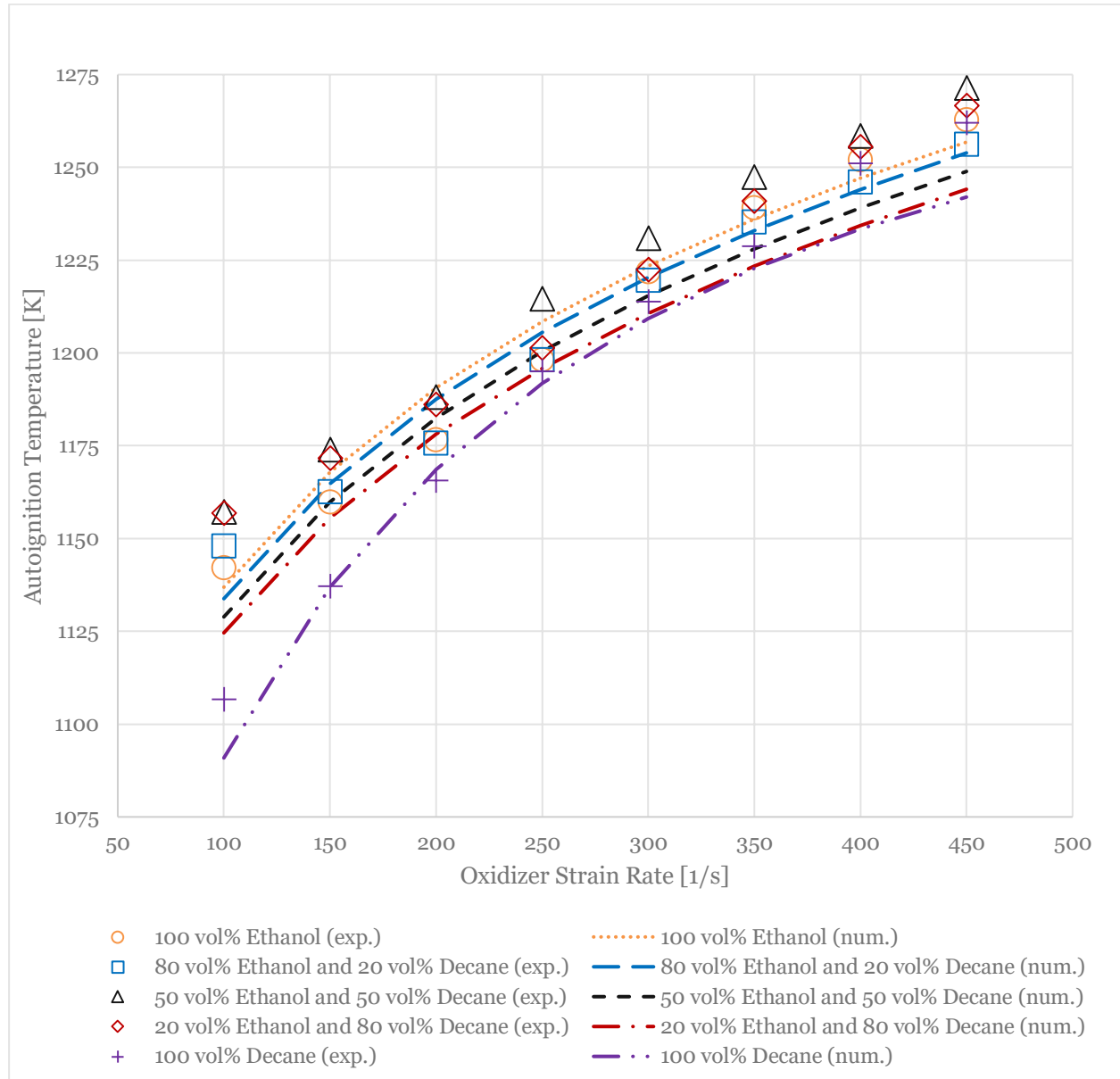


Figure 16: Experimental and numerical autoignition temperatures of the five fuels as a function of the oxidizer strain rate

Generally, the deviation between the experimental and numerical results is within an acceptable range. However, there is a trend that the experimental data are higher than the numerical ones.

For the 100 vol% decane, the results, especially at lower strain rates, are satisfactory. Only at the highest strain rate of 400 and 450, the deviation of the autoignition temperature is almost 20 kelvin.

According to the experiments, it seems that already small shares of ethanol in the mixtures inhibit the low-temperature chemistry of decane. At lower strain rates, the mixtures in the experiments are harder to ignite than the numerical results are showing.

For 100 vol% ethanol and all mixtures of ethanol with decane, it is observed that the experimental values between strain rates of 150 to 250 do not agree with the general trend and the numerical simulation. There seems to be a dip in the general trend. In this area, the overall reactivity of the fuels appears to increase, and the autoignition temperatures drop to a lower level. The simulation for the numerical results is not showing this trend with the dip.

At higher strain rates, Figure 16 shows that the mixture of 50 vol% ethanol and 50 vol% decane and the mixture of 20 vol% ethanol and 80 vol% decane are the hardest to ignite. This is not in agreement with the numerical results. The numerical results show that the higher the ethanol share is, the harder is the fuel to ignite.

In this work, the mixture of 50 vol% ethanol and 50 vol% decane and the mixture of 20 vol% ethanol and 80 vol% decane have the largest deviations from the numerical results in this area of higher strain rates.

To understand why already small shares of ethanol in the mixtures inhibits the low-temperature chemistry of decane, why there is a dip in the general trend at lower strain rates, why the mixture of 50 vol% ethanol and 50 vol% decane and the mixture of 20 vol% ethanol and 80 vol% decane are the hardest to ignite at the high strain rates, and also to validate the experimental data presented here, it would be advantageous to study the chemical relationships of ethanol and decane in more detail by experts in the future. This should lead to a better comprehension of the autoignition behaviors as a function of the strain rate of mixtures with different ethanol decane shares.

The best agreement between experiment and simulation exists for the pure ethanol and the mixture 80 vol% ethanol and 20 vol% decane. There is only a bigger deviation around the strain rates of 150 to 250.

So far, an answer to the deviations between the experimental and numerical results could not be found. Additionally, it is not clear why at the strain rates of 150 to 250, the pure ethanol and the mixtures of ethanol and decane show a dip. The answer could be to adapt the used CounterFlowDiffusionFlame1D solver in OpenSMOKE++ for the numerical simulation or explain this phenomenon by the chemical reaction between ethanol and decane.

Comparison and Discussion Extinction of Results

Since the simulation for the extinction events has not provided any results, this part can only discuss the experimental extinction results.

As analyzed in Chapter 4.1 and presented in Figure 14, there is a trend that the extinction strain rate rises to a higher level at a constant oxygen mass fraction of the oxidizer stream by increasing the ethanol share (especially at lower strain rates).

The mixture of 80 vol% ethanol and 20 vol% decane shows an interesting pattern: The whole increase of the extinction strain rate from oxygen mass fraction of 0.16 to 0.19 is only 65.6. At the same time, the mixture of 50 vol% ethanol and 50 vol% decane has an increase of the strain rate of nearly 129 in this area or the mixture of 20 vol% ethanol and 80 vol% decane, which has an increase of almost 136.

It seems that there is a certain ratio of ethanol and decane in the mixture, which makes it possible to extinguish the flames at strain rates lower than the expected trend.

To learn more about this finding from the experiments, it would be helpful to verify the experimental results with numerical results from a simulation. As mentioned in Chapter 4.2, it is necessary to get a new or extended kinetic mechanism from the CRECK Modeling Group at Politecnico di Milano, making the simulation possible.

By performing and watching the experiments, further insight is found: All the experiments with the mixtures (80 vol% ethanol and 20 vol% decane, 50 vol% ethanol and 50 vol% decane, and 20 vol% ethanol and 80 vol% decane) show the phenomenon that the fuels start to bubble in the fuel cup, see Figure 17. This happens regardless of the current oxygen mass fraction of the oxidizer stream and the strain rate.

The first assumption is that the power of the cooling system is too weak. Therefore, the whole cooling system is improved and adjusted to ensure sufficient cooling of the counterflow burner.



Figure 17: Bubbles on the surface of the mixture 20 vol% ethanol and 80 vol% decane during an extinction experiment with an oxygen mass fraction of 0.19

After the modification of the cooling system, the phenomenon of bubbling is still present. To guarantee that the whole counterflow burner setup in extinction configuration works without any problems and the bubbles are not due to the experimental equipment, another modified mixture is tested: 20 vol% n-heptane and 80 vol% decane. By performing this experiment, no bubbles are on the surface of the fuel, see Figure 18. This mixture shows a smooth surface.

The bubbles also do not appear by testing the pure fuels as 100 vol% ethanol and 100 vol% decane.

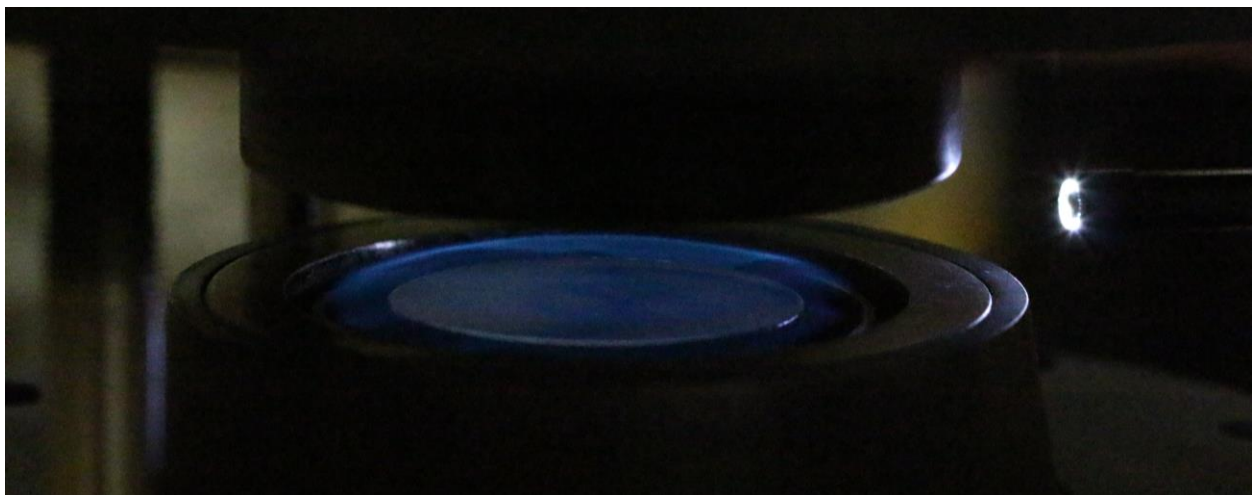


Figure 18: Smooth surface of the mixture 20 vol% n-heptane and 80 vol% decane during an extinction experiment with an oxygen mass fraction of 0.17

That confirms that the cooling system works properly and concludes that mixing ethanol and decane causes a previously unknown reaction that generates bubbles. This phenomenon of bubbles could not be found in previous literature.

To find reasons why this certain mixture of ethanol and decane with different mixing ratios produces such bubbles on the surface of the liquid fuels in the fuel cup, detailed research is needed on this topic.

5 Conclusions

This diploma thesis aims to investigate the critical conditions of autoignition and extinction of five liquid fuels in non-premixed flows with a counterflow burner at atmospheric pressure. The idea is to analyze the experimental data (autoignition temperatures and extinction strain rates) and compare them with numerical data from simulations. The fuels are pure ethanol, three mixtures of ethanol with decane (80 vol% ethanol and 20 vol% decane, 50 vol% ethanol and 50 vol% decane, and finally 20 vol% ethanol and 80 vol% decane), and pure decane.

All autoignition results display that increasing the strain rate makes the fuels harder to ignite and increases the autoignition temperature. Furthermore, the results indicate that pure decane always has the lowest autoignition temperature. Whereas the higher the decane share is in the mixture, the higher is the autoignition temperature, especially at lower strain rates.

By mixing ethanol and decane, it seems that already small shares of ethanol in the mixtures inhibit the low-temperature chemistry of decane. That means at lower strain rates, mixtures with a small share of ethanol are harder to ignite in the experiments than the numerical results predict.

At higher strain rates, the mixture of 50 vol% ethanol and 50 vol% decane and the mixture of 20 vol% ethanol and 80 vol% decane are the hardest to ignite. This does not agree with the numerical results where pure ethanol is always the hardest fuel to ignite.

Further research, especially on the chemical relationships between ethanol and decane, is needed to learn more about these findings and better comprehend the autoignition behaviors of mixtures of ethanol and decane.

For the investigation of extinction, it is impossible to compare experimental and numerical results. Since the used kinetic mechanism does not support the simulation of liquid fuels. To get numerical results in future studies, it is necessary to get a new or extended numerical formulation.

All the experimental extinction results show that the higher the oxygen mass fraction of the oxidizer stream, the higher is the extinction strain rate, regardless of the fuel.

Additionally, there is a trend in the results that with higher ethanol content in the fuel, the strain rate increases at a constant oxygen mass fraction of the oxidizer stream.

However, the mixture of 80 vol% ethanol and 20 vol% decane does not follow this general trend, especially at higher strain rates where the extinction strain rate comes even closer to the result of 100 vol% decane. It seems that a certain ratio of ethanol and decane leads to lower strain rates than the expected trend. This ratio of ethanol and decane could also be part of upcoming studies.

During the experiments with the mixtures of ethanol and decane, bubbles occur on the surface of the fuel. This phenomenon is not yet known in the literature and must be researched in more detail.

Appendix

The results of the autoignition and extinction experiments shown are arithmetically averaged values from all experimental runs.

Autoignition Results

To calculate the experimental gas temperature T_g , all missing values of variables are inserted into Equation (4-6). Then the equation looks like Equation (A-1). This equation determines the actual gas temperature T_g including the radiant correction depending on the measured temperature of the thermocouple T_{tc} and the strain rate a_2 .

$$T_g = T_{tc} + 0.2 \frac{5.67 \cdot 10^{-8} (T_{tc}^4 - 295.15^4)}{0.0759 \left(0.24 + 0.56 \left(\frac{a_2 \cdot 0.0105 \cdot 0.0002}{0.000158} \right)^{0.45} \right)} \quad (\text{A-1})$$

However, Equation (A-1) does not provide the exact results. The values for the thermal conductivity k and the viscosity ν are for an air oxidizer stream temperature of 1200 kelvin. Interpolation is required for the exact results, as shown by the code in Figure 19.

```
def CORTEMP(Ttc, a2):
    Tp = Ttc
    L = 10.5e-3          #Separation distance [m]
    d = 2e-4            #Diameter thermocouple [m]
    T1 = 973            #Temperature 1 for interpolation [K]
    T2 = 1273           #Temperature 2 for interpolation [K]
    niu1 = 1.133e-4     #Viscosity of oxidizer stream at T1 [m²/s]
    niu2 = 1.529e-4     #Viscosity of oxidizer stream at T2 [m²/s]
    k1 = 6.581e-2       #Thermal conductivity at T1 [W/mK]
    k2 = 7.465e-2       #Thermal conductivity at T2 [W/mK]
    Etc = 0.2           #Emissivity of Type R thermocouple [-]
    sigma = 5.67e-8     #Stefan-Boltzmann constant[W/m²K⁴]
    Tw = 295.15         #Temperature of surroundings [K]
    V2 = (a2 * L) / 2   #Flow velocity of oxidizer stream at boundary [m/s]
    while true:
        niu = niu1 + (Tp - T1) / (T2 - T1) * (niu2 - niu1) #Interpolation for niu at Tp
        k = k1 + (Tp - T1) / (T2 - T1) * (k2 - k1)          #Interpolation for k at Tp
        Re = (V2 * d) / niu                                  #Reynolds number [-]
        Nu = (0.24 + 0.56 * Re**0.45)                       #Nusselt number [-]
        Tg = Ttc + Etc * sigma * (Ttc**4 - Tw**4) * d / (k * Nu) #Gas temperature [K]
        if abs(Tg - Tp) <= 0.1:
            break
        else:
            Tp = Tg
    return Tg
```

Figure 19: Code for the interpolation to calculate the exact experimental autoignition temperature

100 vol% Ethanol

Strain rate a_2 [1/s]	100	150	200	250	300	350	400	450
Oxygen mass fraction [-]	0.233	0.233	0.233	0.233	0.233	0.233	0.233	0.233
Temperature of thermocouple T_{tc} [K]	1082.7	1103.5	1121.9	1143.5	1166.3	1183.4	1196.6	1207.7
Radiant correction [K]	+59.2	+56.2	+54.6	+54.6	+55.4	+55.6	+55.4	+55.1
Gas temperature T_g [K]	1142.0	1159.7	1176.5	1198.1	1221.8	1239.0	1252.0	1262.8
Numerical autoignition temperature [K]	1136.9	1167.9	1190.6	1208.5	1223.4	1236.0	1247.1	1256.8

80 vol% Ethanol and 20 vol% Decane

Strain rate a_2 [1/s]	100	150	200	250	300	350	400	450
Oxygen mass fraction [-]	0.233	0.233	0.233	0.233	0.233	0.233	0.233	0.233
Temperature of thermocouple T_{tc} [K]	1087.6	1105.9	1121.1	1143.5	1164.4	1180.2	1191.5	1202.1
Radiant correction [K]	+60.3	+56.7	+54.5	+54.6	+55.1	+55.0	+54.5	+54.1
Gas temperature T_g [K]	1147.9	1162.6	1175.6	1198.1	1219.5	1235.2	1246.0	1256.1
Numerical autoignition temperature [K]	1133.8	1164.8	1187.5	1205.5	1220.3	1233.0	1244.0	1253.9

50 vol% Ethanol and 50 vol% Decane

Strain rate a_2 [1/s]	100	150	200	250	300	350	400	450
Oxygen mass fraction [-]	0.233	0.233	0.233	0.233	0.233	0.233	0.233	0.233
Temperature of thermocouple T_{tc} [K]	1095.2	1115.3	1131.5	1157.3	1174.1	1190.5	1202.1	1215.0
Radiant correction [K]	+61.9	+58.6	+56.5	+57.2	+56.9	+56.9	+56.4	+56.4
Gas temperature T_g [K]	1157.1	1173.9	1188.0	1214.5	1230.9	1247.4	1258.5	1271.3
Numerical autoignition temperature [K]	1128.9	1159.9	1182.5	1200.5	1215.4	1228.0	1239.1	1248.9

20 vol% Ethanol and 80 vol% Decane

Strain rate a_2 [1/s]	100	150	200	250	300	350	400	450
Oxygen mass fraction [-]	0.233	0.233	0.233	0.233	0.233	0.233	0.233	0.233
Temperature of thermocouple T_{tc} [K]	1095.0	1113.4	1129.9	1146.2	1166.9	1185.0	1199.6	1211.0
Radiant correction [K]	+61.9	+58.2	+56.1	+55.1	+55.5	+55.9	+55.9	+55.7
Gas temperature T_g [K]	1156.9	1171.6	1186.0	1201.3	1222.4	1240.9	1255.6	1266.6
Numerical autoignition temperature [K]	1124.6	1155.5	1178.1	1195.9	1210.7	1223.4	1234.3	1244.1

100 vol% Decane

Strain rate a_2 [1/s]	100	150	200	250	300	350	400	450
Oxygen mass fraction [-]	0.233	0.233	0.233	0.233	0.233	0.233	0.233	0.233
Temperature of thermocouple T_{tc} [K]	1053.3	1084.6	1112.7	1140.9	1159.7	1174.8	1195.7	1206.9
Radiant correction [K]	+53.3	+52.6	+52.9	+54.1	+54.2	+54.0	+55.3	+55.0
Gas temperature T_g [K]	1106.6	1137.2	1165.6	1195.0	1213.9	1228.8	1251.0	1261.9
Numerical autoignition temperature [K]	1090.9	1136.9	1168.6	1191.8	1209.3	1222.8	1233.4	1242.0

Extinction Results

100 vol% Ethanol

Oxygen mass fraction [-]	0.15	0.16	0.17	0.18	0.19
Experimental strain rate a_2 [1/s]	67.3	99.3	140.3	197.0	265.3
Numerical strain rate a_2 [1/s]	Not determinable with solver used				

80 vol% Ethanol and 20 vol% Decane

Oxygen mass fraction [-]	0.15	0.16	0.17	0.18	0.19
Experimental strain rate a_2 [1/s]	65.3	83.2	95.8	115.0	149.0
Numerical strain rate a_2 [1/s]	Not determinable with solver used				

50 vol% Ethanol and 50 vol% Decane

Oxygen mass fraction [-]	0.15	0.16	0.17	0.18	0.19
Experimental strain rate a_2 [1/s]	43.7	55.5	80.0	134.0	184.0
Numerical strain rate a_2 [1/s]	Not determinable with solver used				

20 vol% Ethanol and 80 vol% Decane

Oxygen mass fraction [-]	0.15	0.16	0.17	0.18	0.19
Experimental strain rate a_2 [1/s]	-*	59.5	88.3	129.0	195
Numerical strain rate a_2 [1/s]	Not determinable with solver used				

* Impossible to determine with used experimental setup

100 vol% Decane

Oxygen mass fraction [-]	0.15	0.16	0.17	0.18	0.19
Experimental strain rate a_2 [1/s]	-*	42.0	63.3	95.7	151.0
Numerical strain rate a_2 [1/s]	Not determinable with solver used				

* Impossible to determine with used experimental setup

References

- [1] INTERNATIONAL ENERGY AGENCY: *Global EV Outlook 2021*. URL <https://www.iea.org/reports/global-ev-outlook-2021>. - accessed 2021-06-18. — IEA
- [2] KONDRATIEV, VICTOR N.: *Combustion*. URL <https://www.britannica.com/science/combustion>. - accessed 2021-06-17. — Encyclopedia Britannica
- [3] WINTERBONE, DESMOND E. ; TURAN, ALI: Combustion and Flames. In: *Advanced Thermodynamics for Engineers*. Oxford, United Kingdom : Elsevier, 2015 — ISBN 978-0-444-63373-6, S. 323–344
- [4] GEHMLICH, RYAN K.: *Experimental Studies on Nonpremixed Combustion at Atmospheric and Elevated Pressures*. San Diego, U.S., University of California, San Diego, 2015
- [5] SHAN, RUIQIN ; LU, TIANFENG: Ignition and extinction in perfectly stirred reactors with detailed chemistry. In: *Combustion and Flame* Bd. 159 (2012), Nr. 6, S. 2069–2076
- [6] GLASSMAN, IRVIN ; YETTER, RICHARD A. ; GLUMAC, NICK G.: Diffusion flames. In: *Combustion*. Oxford, United Kingdom : Academic Press, 2015 — ISBN 978-0-12-407913-7, S. 301–361
- [7] FISHER, ELIZABETH M. ; WILLIAMS, BRADLEY A. ; FLEMING, JAMES W.: Determination of the Strain in Counterflow Diffusion Flames From Flow Conditions. In: *Proceedings of the Eastern States Section of the Combustion Institute* (1997), S. 191–194
- [8] TAYLOR, SIMON C.: *Burning Velocity and the Influence of Flame Stretch*. Leeds, United Kingdom, University of Leeds, 1991
- [9] SHIH, HSIN-YI: Computed extinction limits and flame structures of H₂/O₂ counterflow diffusion flames with CO₂ dilution. In: *International Journal of Hydrogen Energy* Bd. 34 (2009), Nr. 9, S. 4005–4013
- [10] CAREY, FRANCIS A.: *Hydrocarbon*. URL <https://www.britannica.com/science/hydrocarbon>. - accessed 2021-05-28. — Encyclopedia Britannica
- [11] KOPP, OTTO C.: *Fossil Fuel*. URL <https://www.britannica.com/science/fossil-fuel>. - accessed 2021-06-01. — Encyclopedia Britannica

- [12] ALTERNATIVE FUELS DATA CENTER: *Alternative Fuel Definition and Specifications*. URL <https://afdc.energy.gov/laws/9218>. - accessed 2021-06-01. — U.S. Department of Energy
- [13] PUBCHEM: *PubChem Compound Summary for CID 702, Ethanol*. URL <https://pubchem.ncbi.nlm.nih.gov/compound/702>. - accessed 2021-06-03. — National Center for Biotechnology Information
- [14] WADE, LEROY G.: *Alcohol*. URL <https://www.britannica.com/science/alcohol>. - accessed 2021-06-02. — Encyclopedia Britannica
- [15] SARATHY, S. MANI ; OßWALD, PATRICK ; HANSEN, NILS ; KOHSE-HÖINGHAUS, KATHARINA: Alcohol combustion chemistry. In: *Progress in Energy and Combustion Science* Bd. 44 (2014), S. 40–102
- [16] PUBCHEM: *PubChem Compound Summary for CID 15600, Decane*. URL <https://pubchem.ncbi.nlm.nih.gov/compound/15600>. - accessed 2021-06-03. — National Center for Biotechnology Information
- [17] SEISER, REINHARD ; SESHADRI, KALYANASUNDARAM ; PISKERNIK, EDGAR ; LIÑÁN, AMABLE: Ignition in the viscous layer between counterflowing streams: asymptotic theory with comparison to experiments. In: *Combustion and Flame* Bd. 122 (2000), Nr. 3, S. 339–349
- [18] SESHADRI, KALYANASUNDARAM ; WILLIAMS, FORMAN A.: Laminar flow between parallel plates with injection of a reactant at high reynolds number. In: *International Journal of Heat and Mass Transfer* Bd. 21 (1978), Nr. 2, S. 251–253
- [19] LIÑÁN, AMABLE: The asymptotic structure of counterflow diffusion flames for large activation energies. In: *Acta Astronautica* Bd. 1 (1974), Nr. 7–8, S. 1007–1039
- [20] FENDELL, FRANCIS E.: Ignition and extinction in combustion of initially unmixed reactants. In: *Journal of Fluid Mechanics* Bd. 21 (1965), Nr. 02, S. 281–303
- [21] PANDYA, TEJAL P. ; WEINBERG, FELIX J.: The Structure of Flat, Counter-Flow Diffusion Flames. In: *Proceedings of the Royal Society of London. Series A, Mathematical and Physical Sciences* Bd. 279 (1964), Nr. 1379, S. 544–561
- [22] SESHADRI, KALYANASUNDARAM ; HUMER, STEFAN ; SEISER, REINHARD: Activation-energy asymptotic theory of autoignition of condensed hydrocarbon fuels in non-premixed flows with comparison to experiment. In: *Combustion Theory and Modelling* Bd. 12 (2008), Nr. 5, S. 831–855
- [23] NIEMANN, ULRICH ; SESHADRI, KALYANASUNDARAM ; WILLIAMS, FORMAN A.: Accuracies of laminar counterflow flame experiments. In: *Combustion and Flame* Bd. 162 (2015), Nr. 4, S. 1540–1549

- [24] FALSETTI, CHIARA ; KAPULLA, RALF ; PARANJAPE, SIDHARTH ; PALADINO, DOMENICO: Thermal radiation, its effect on thermocouple measurements in the PANDA facility and how to compensate it. In: *Nuclear Engineering and Design* Bd. 375 (2021), S. 111077
- [25] SCHASCHKE, CARL: *A Dictionary of Chemical Engineering*. Oxford, United Kingdom : Oxford University Press, Incorporated, 2014 — ISBN 978-0-19-100269-4
- [26] CHOUDER, AISSA ; SILVESTRE, SANTIAGO ; TAGHEZOUT, BILAL ; KARATEPE, ENGIN: Monitoring, modelling and simulation of PV systems using LabVIEW. In: *Solar Energy* Bd. 91 (2013), S. 337–349
- [27] SHADDIX, CHRISTOPHER R.: Correcting thermocouple measurements for radiation loss: A critical review. In: *33rd National Heat Transfer Conference*. Albuquerque, New Mexico, U.S., 1999, S. 1–10
- [28] SHADDIX, CHRISTOPHER R.: A new method to compute the proper radiant heat transfer correction of bare-wire thermocouple measurements. In: *10th U. S. National Combustion Meeting*. College Park, Maryland, U.S., 2017, S. 1–6
- [29] MODEST, MICHAEL F.: Fundamentals of Thermal Radiation. In: *Radiative Heat Transfer*. Third Edition. Oxford, United Kingdom : Elsevier, 2013 — ISBN 978-0-12-386944-9, S. 1–30
- [30] GASKELL, DAVID R.: *An Introduction to Transport Phenomena in Materials Engineering*. Bd. Second Edition. New York, U.S. : Momentum Press, 2012 — ISBN 978-1-60650-355-3
- [31] CUOCI, ALBERTO ; FRASSOLDATI, ALESSIO ; FARAVELLI, TIZIANO ; RANZI, ELISEO: OpenSMOKE++: An object-oriented framework for the numerical modeling of reactive systems with detailed kinetic mechanisms. In: *Computer Physics Communications* Bd. 192 (2015), S. 237–264
- [32] CRECK MODELING LAB OF POLITECNICO DI MILANO: *C1-C16 HT+LT mechanism (Version 2003, March 2020)*. URL <http://creckmodeling.chem.polimi.it/menu-kinetics/menu-kinetics-detailed-mechanisms/107-category-kinetic-mechanisms/403-mechanisms-1911-tot-ht-lt>. - accessed 2021-06-29. — Kinetic mechanisms - CRECK Modeling Lab

List of Equations

Equation (2-1): Oxidizer strain rate at stagnation plane.....	10
Equation (2-2): Normal components of the flow velocity of oxidizer stream	10
Equation (2-3): General Damköhler number.....	11
Equation (4-1): Convection-radiation energy balance.....	27
Equation (4-2): Nusselt number	27
Equation (4-3): Gas temperature depending on Nusselt number	27
Equation (4-4): Nusselt number for cylindric problems	27
Equation (4-5): Reynolds number	28
Equation (4-6): Gas temperature with all parameters inserted.....	28
Equation (A-1): Gas temperature with all values of parameters inserted.....	i

List of Figures

Figure 1: Schematic illustration of a diffusion flame generated by a counterflow burner [9].....	5
Figure 2: S-shaped curve –maximum temperature in the reaction zone as a function of the Damköhler number [4].....	12
Figure 3: Schematic illustration of the entire experimental setup for the autoignition and extinction experiments	14
Figure 4: Schematic illustration of the autoignition configuration of the counterflow burner – figure slightly modified from [22].....	16
Figure 5: Schematic cutaway view of the counterflow configuration for autoignition experiments – figure slightly modified from [4].....	17
Figure 6: Counterflow burner in autoignition configuration at the University of California, San Diego.....	17
Figure 7: Schematic drawing of the upper part of the counterflow burner in extinction configuration – figure excerpt from [23].....	18
Figure 8: Counterflow burner in extinction configuration at the University of California, San Diego.....	19
Figure 9: Type R thermocouple between the lower and upper part of the counterflow burner.....	20
Figure 10: LabVIEW™ user interface during an autoignition event of 100 vol% ethanol at a strain rate of 100.....	21
Figure 11: High-speed image of an autoignition event of 100 vol% decane at a strain rate of 100	24
Figure 12: High-speed image of an extinction event of 20 vol% ethanol and 80 vol% decane at an oxygen mass fraction of 0.17.....	25
Figure 13: Corrected and averaged experimental autoignition temperatures of the five fuels as a function of the oxidizer strain rate	30
Figure 14: Averaged experimental extinction strain rates of the five fuels as a function of the oxygen mass fraction of the oxidizer stream.....	32
Figure 15: Numerical autoignition temperatures of the five fuels as a function of the oxidizer strain rate.....	34

Figure 16: Experimental and numerical autoignition temperatures of the five fuels as a function of the oxidizer strain rate	36
Figure 17: Bubbles on the surface of the mixture 20 vol% ethanol and 80 vol% decane during an extinction experiment with an oxygen mass fraction of 0.19	39
Figure 18: Smooth surface of the mixture 20 vol% n-heptane and 80 vol% decane during an extinction experiment with an oxygen mass fraction of 0.17	39
Figure 19: Code for the interpolation to calculate the exact experimental autoignition temperature	i

List of Tables

Table 1: Structures of representative hydrocarbons	6
Table 2: Properties of ethanol [13]	7
Table 3: Properties of decane [16]	9
Table 4: Overview of investigated fuels	13
Table 5: Variables to calculate correction of thermocouple temperature at assumed air oxidizer stream temperature of 1200 kelvin [27] [29] [30]	29

Affidavit

I declare in lieu of oath, that I wrote this thesis and performed the associated research myself, using only literature cited in this volume. If text passages from sources are used literally, they are marked as such.

I confirm that this work is original and has not been submitted elsewhere for any examination, nor is it currently under consideration for a thesis elsewhere.

I acknowledge that the submitted work will be checked electronically-technically using suitable and state-of-the-art means (plagiarism detection software). On the one hand, this ensures that the submitted work was prepared according to the high-quality standards within the applicable rules to ensure good scientific practice "Code of Conduct" at the TU Wien. On the other hand, a comparison with other student theses avoids violations of my personal copyright.

San Diego, September 2021

Simon Leu